ELSEVIER

PII: S0032-3861(96)00702-1

Polymer Vol. 38 No. 8, pp. 1787–1808, 1997

0032-3861/97/$17.00 + 0.00

Evolution of morphology in compatibilized vs uncompatibilized polyamide blends

B. Majumdar*
Corporate Research Process Technologies Laboratory, 3M, St. Paul, MN 55144-1000, USA

and D. R. Paul† and A. J. Oshinski
Department of Chemical Engineering and Center for Polymer Research, University of Texas at Austin, Austin, TX 78712, USA
(Received 17 April 1996)

The development of phase morphology in non-reactive vs reactive polyamide blends with a styrene–acrylonitrile (SAN) copolymer and SEBS (a styrenic triblock copolymer with ethylene–butylene midblocks) in a co-rotating twin screw extruder was investigated using electron microscopy techniques. For the polyamide/SAN systems, significant differences were observed between the evolution of morphology in non-reactive binary blends vs blends compatibilized with a reactive imidized acrylic (IA) polymer which is miscible in the SAN phase and has functional groups which are capable of reacting with the amine end groups in the polyamide phase. While a steady decrease in the dispersed phase particle size was observed in general for the non-reactive nylon 6/SAN blends with both increasing screw length and speed, for the ternary nylon 6/SAN/IA blends a dramatic drop in the dispersed phase particle size was observed in the initial region of the screw almost immediately after melting of the pellets followed by some coalescence of dispersed phase in the latter stages leading to a dual population of particle at the exit of the extruder. The extent and onset of coalescence after attainment of minimum particle size in the initial region of the screw in reactive nylon 6/SAN blends was found to be strongly dependent on the screw speed and configuration. The extent of chemical reaction along the extruder screw for reactive nylon 6/SAN blends was dependent on the screw speed, extruder configuration and flow rate. While similar differences in the evolution of morphology were observed between non-reactive and reactive polyamide/SEBS systems, changing the polyamide type from monofunctional (nylon *x*, e.g. nylon 6) to difunctional (nylon *x*, *y*, e.g. nylon 6,6) revealed interesting differences even within these reactive blends. Significant differences in both the development of morphology and reaction profile along the screw were also observed between binary and ternary nylon 6/rubber blends containing similar concentrations of reactive maleic anhydride functionality in the rubber phase using a fixed screw speed and configuration.

(Keywords: blends; morphology; polyamide)

INTRODUCTION

The control of morphology in multiphase polymer blends using reactive compatibilization has been described in several recent publications[1–13]. Previous work has demonstrated that in addition to process and rheological issues, some critical chemical factors that influence the formation of block or graft copolymers *in situ* via interfacial reaction during the melt blending process include the type of functional groups incorporated, the manner in which they are incorporated (grafted, comonomer or terminal groups), molecular architecture, spacing and concentration of these functional groups, molecular weight of the chain to which the functional groups are attached and the physical interaction of the functional polymer with the major components of the blend[1–13]. The work described here is motivated by our interest in the evolution and stability of blend morphology generated via interfacial reactions in polyamide systems in flow fields that exist inside typical industrial mixing devices, viz. a co-rotating twin screw extruder. This study compares the morphology generation in uncompatibilized vs reactively compatibilized multiphase blends based on nylon 6 and styrene–acrylonitrile (SAN) copolymer[6–9], and nylon 6 and styrene/ethylene–butene/styrene triblock copolymer (SEBS)[10–13]. Although both systems have been compatibilized very effectively using appropriate reactive agents in our previous work[6–13], there are still some important but unanswered questions related to the generation of morphology and its stability, during the extrusion process.

An effective strategy for compatibilizing nylon/SAN blends is the addition of a polymer which is miscible with the SAN phase that can react with the amine end-groups of the nylon phase[6–9,14]. We described in a series of recent papers the effectiveness of imidized acrylic polymers for controlling morphology in nylon 6/SAN blends (no rubber phase) which serves as a simplified version of the commercially attractive nylon 6/ABS alloy system. These imidized acrylic polymers were

* Present address: General Electric Co., One Noryl Ave., Selkirk, NY 12158, USA
† To whom correspondence should be addressed

synthesized via reactive extrusion of methylamines with poly(methyl methacrylate) to produce materials with at least four different types of chemical repeat units[6,15–17]. In addition to generating methyl glutarimide units, this process leads to small amounts of methacrylic acid and glutaric anhydride units plus some methyl methacrylate units that remain unchanged. The acid and anhydride groups provide chemical functionality for reaction with the polyamide. By controlling the amount of acid and anhydride in the imidized acrylic polymers through a re-esterification process[15,17], it is possible to preserve their miscibility with SAN copolymers over a limited range of AN contents[6,16].

It has been demonstrated in our recent work with nylon/maleated SEBS (SEBS-*g*-MA) blends that the particle size can be varied through two orders of magnitude by only changing the extent of graft copolymer formed at the polymer–polymer interface while maintaining the same processing conditions[10–13]. It has been also proposed that the topology of grafting plays a critical role in determining the final morphology of the blend[10,12]. In the case of blends of SEBS-*g*-MA with polyamide chains that contain two amine ends, i.e. difunctional, complex particles were observed which may be attributed to 'crosslinking' type effects developed through two particle attachments per chain possible in difunctional polyamides, while for monofunctional polyamides (one amine end per chain) one point attachments apparently led to much smaller spherical particles[10–13].

This paper addresses some important issues related to the evolution of morphology stemming from the competition between drop break-up and coalescence for both non-reactive and reactive blends in a fully intermeshing co-rotating twin screw extruder with segmented screw design. The extruder used is a 'clamshell' type to facilitate rapid sampling along the screw for both electron microscopy and chemical analysis. In previous studies, the morphology of the same systems was examined at the exit of a single screw extruder outfitted with an intensive mixing head[6,10]. The current study explores the progression of morphology in relation to the extent of chemical reaction between the functional species in the two phases. In particular, we will focus on the effectiveness of the graft copolymer formed at the interface during the melt mixing for stabilizing the dispersed phase morphology against coalescence in typical flow fields which exists inside such a processing device.

BACKGROUND

The first attempts to quantify drop break-up and coalescence in multiphase fluid systems can be traced back to the first half of this century[18–21] and have been followed by numerous efforts over the last three decades to understand factors that control morphology in multiphase fluid systems[18–62]. Most of the initial activity dealt with simple Newtonian systems[18,19,22–26]. Over the last two decades viscoelastic systems have come to the forefront of research activity[27–38] due to widespread interest in the control of morphology in multiphase polymer systems as a means to manipulate the properties of these materials.

Drop break-up in polymer blends

The seminal work by Taylor over six decades ago[18,19] on drop break-up in Newtonian systems in a simple shear field has been the basis for investigation of more complex systems and flow-fields. Taylor's analysis considers how the balance of shear and interfacial forces affect drop dimensions and stability with results expressed in terms of the so-called capillary number,

$$Ca = G\eta_m D/2\gamma$$

and the viscosity ratio, $\eta_r = \eta_d/\eta_m$ where D is the diameter of the drop, G is the shear rate, η_m is the matrix viscosity, η_d is the dispersed phase viscosity, and γ is the interfacial tension. Drop break-up is predicted to occur only when the viscosity ratio is less than 2.5. Several subsequent studies for Newtonian systems in both shear and extensional flow have reached qualitatively similar conclusions[22–25,28]. It was pointed out, however, that drop break-up was possible over a wider range of viscosity ratios in extensional flow for Newtonian systems[28–30,34,35]. Van Oene[27] was one of the first investigators to point out the limitations of extending such analyses to viscoelastic systems like polymer blends in which the individual components could have large normal stresses in flow type situations[27,31].

The final morphology of a blend represents the balance of the drop break-up and coalescence rates at the end of the mixing process. Most attempts at correlating particle size from such processes are expressed in terms of the capillary number and viscosity ratio which emerge from the Taylor analysis without explicitly accounting for the coalescence process. A frequently cited example is the results from an extensive study by Wu[37] that are expressed by

$$(G\eta_m D)/(\gamma) = 4(\eta_r)^{\pm 0.84}$$

These results were developed from experimental data on polyamide and polyester blends which contained 15% ethylene–propylene rubbers as the dispersed phase. Wu's correlation implies a minimum particle size when the viscosities of the two phases are closely matched. Several researchers have examined the validity of this correlation for polymer blends. While Serpe *et al.*[38] claimed a general agreement with Wu's results in their experimental observations, other investigators[56,57,63] have pointed out some discrepancies between their experimental observations regarding the dependence of particle size on the viscosity ratio, η_r, and the correlations proposed by Wu. Also, the inverse relationship proposed by Wu between particle size and shear rate has come under scrutiny in recent years. Sundararaj *et al.*[58] recently observed an experimental minimum in the dispersed phase particle size with increasing shear rates which they attributed to a higher elasticity of the droplet and, hence, increased resistance to deformation at increased shear rates. More recently, Fortenly and Zivny[49,50] have developed a theoretical framework which predicts that in concentrated systems the dependence of droplet size on shear rate is strongly determined by the material properties of the blend components and can be either an increasing, a decreasing, or a non-monotonic function of the shear rate.

Coalescence in polymer blends

Flow induced coalescence in Newtonian systems has been a subject of considerable research activity for the last eight decades since the pioneering work of

Smoluchowski on aqueous colloid solutions[20,21]. While collision and coalescence probability can be predicted with a reasonable degree of certainty in Newtonian systems[39–42], only crude estimates are available at present for viscoelastic systems like polymer blends[43–59]. A major incentive for investigating coalescence phenomenon in viscoelastic media has been consistent experimental reports from different laboratories of observations of a significantly larger domain size in polymer blends than that predicted by the Taylor theory even at relatively low concentrations (<5%) of the dispersed phase[44–58,61]. Several researchers have attempted to account for this discrepancy by developing population balance models[39–42] which take into account the competition between drop break-up and coalescence during the mixing process. While, in general, these models predict an increase in phase size with dispersed phase concentration owing to the increased probability of collisions as the number density of particles increases, they still seriously underestimate the degree of coalescence that is experimentally observed during mixing processes in polymer blends[43–56]. In fact, some of the same factors that supposedly favour drop break-up (e.g. high shear rates, reduced dispersed phase viscosity) have been experimentally observed to actually increase coalescence in polymer blends[52,53,57,58].

Effect of compatibilization on drop-break up, coalescence and steric stabilization

Interfacial agents in the form of premade block and/or graft copolymers have been used to control phase morphology in polymer blends for over three decades[61–78]. Both experimental observations[68–74] and theoretical predictions[75–78] indicate a reduction in the interfacial tension between immiscible phases in polymer blends and a consequent reduction in the dispersed phase domain size. In addition, the presence of the block or graft copolymers at the interface broadens the interfacial region through penetration of the copolymer chains into the adjacent phases[69,70]. Similar effects result when block or graft copolymers are generated *in situ* during the process of melt mixing through reaction between chemical functionalities available in the polymer chains[1,5,10].

Perhaps more important than the reduction in interfacial tension is the stabilization against coalescence during the mixing process also caused by the location of the copolymer at the interface[1,10,58–62,78]. A significant amount of work has been done to understand this steric stabilization phenomenon in colloids and polymer solutions[79–91]; however, only a small body of literature relates the significance of this effect in polymer blends. Although some investigators have attempted to classify polymer interfaces as mobile, immobile and partially mobile depending on the movement of the dispersed phase with respect to the matrix[44,60], numerous key questions regarding the effectiveness of graft copolymers in stabilizing dispersed phase morphology in polymer blends in flow fields which exist in an extruder still remain unanswered. Some very recent observations by Sondergaard and Lyngaae-Jorgensen using a combination of light scattering and transmission electron microscopy (TEM) in a rheo-optical set-up suggest that significant flow-induced coalescence can occur even in compatibilized systems at sufficiently high shear rates and long time scales[52,53]. In their experiments, while extensive coalescence was observed for binary PS/PMMA blends even at low shear rates ($\sim 0.03\,s^{-1}$), the PS/PMMA blends compatibilized with a PS/PMMA block copolymer demonstrated marked coalescence only at much higher shear rates ($>85\,s^{-1}$) and longer time scales.

Evolution of polymer blend morphology in industrial mixers

A number of studies have monitored the morphology of polymer blends as a function of time in both static mixers and extruders[55,56,92–107]. Macosko and collaborators[95–97,99] have investigated morphology development in static mixtures and conclude that initial stages of mixing involve shearing of the phases into ribbon or sheet structures which is followed by shear and interfacial tension driven breakup of these structures into spherical droplets. Several investigators have also attempted to monitor morphology generation along the length of the extruder screws of various configurations[55,56,99–105] and in general have observed a steady reduction in the dispersed phase particle size along the length of the screw for extruders that contained a typical combination of conveying, shearing and mixing elements. Both Utracki and White report a dramatic increase in the efficiency of dispersive mixing in kneading block sections which create a pressurized situation inside the extruder[55,56,103]. Both studies, however, have focused on highly incompatible systems in the absence of compatibilizers and the minimum particle size reported at the exit of the extruder is $\sim 1\,\mu m$. De Loor *et al.*[105], on the other hand, observed a substantial increase in the dispersed phase particle size due to the presence of intensive mixing elements (kneading blocks) towards the latter stages of the extruder for a more compatible polyolefin-based system in which the minimum particle size reported along the extruder screw was $\sim 0.4\,\mu m$. De Loor *et al.* also reported an increase in the final particle size with an increase in screw speed from 100 to 175 rpm. The authors are aware of only one study of morphology analysis along the extruder screw for a reactively compatibilized system; this is the work of Nishio *et al.*[107] who reported rapid establishment of the final morphology in a reactive nylon/maleated polypropylene system where the dispersed phase particle size remained constant at a sub-micron level beyond the initial stages of the extruder.

Majumdar *et al.*[108] reported in a recent paper a systematic study of the final morphology in reactively compatibilized blends prepared in single screw vs co-rotating twin screw extruders. In most cases the differences in morphology were not very significant demonstrating that even moderate mixing provided by a single screw extruder is sufficient for the amine–anhydride chemical reaction between monofunctional polyamide chains and the functional groups attached to the elastomeric phase to be accomplished to lower the interfacial tension between the two immiscible phases; this is not the case, however, for difunctional polyamides. More recently, Polance and Jayraman[109] have pointed out some of the advantages that a twin screw extruder offers over a single screw extruder through the availability of modular sections which can be optimized for reactive systems. For example, by changing the stagger of kneading discs in a twin screw extruder more flow can be produced in either the forward or reverse

direction thus influencing the residence time of the extrudate. Also, the degree of fill in various parts of the extruder can be influenced by changing the staggering angle of the kneading discs. Thus, twin screw extruders offer significant versatility in processing of reactive systems by allowing for the introduction of non-linearities in the flow profile as opposed to single screw extruders where the flow is more monotonic.

Morphology in reactively compatibilized polyamide blends

Polyamides are an attractive class of polymers for engineering applications but have a number of deficiencies for certain applications, for example brittleness, high moisture sorption, poor dimensional stability and marginal heat deflection temperature. Since the early 1960s numerous efforts have resulted in hundreds of patents and publications describing modification of polyamides for reducing some of these deficiencies. A significant number of these are based on the fact that nylons have inherent chemical functionality (through the amine or carboxyl end groups and potentially through the amide linkage itself) which are capable of reacting with functional species (e.g. maleic anhydride) chemically attached to a second phase with which it is blended. Several of these studies have demonstrated the importance of controlling the dispersed phase particle size in polyamide based blends for generation of an optimized set of properties[10,13,110–115].

A slightly different strategy which has been described in some detail in recent publications involves compatibilizing blends of polyamides with a second immiscible phase by introduction of a compatibilizer precursor that is physically miscible with this second phase but has chemical functionality to react with the polyamide phase[6–9,14]. The idealized situation for this to occur is demonstrated in *Figure 1* where the compatibilizer species C is miscible with the second phase, B, and has functional groups, F, which are capable of forming linkages with the nylon chains at the interface[6–8]. This situation is expected to lead to an efficient reduction in the dispersed phase domain size through a reduction in interfacial tension and an increased resistance to coalescence through steric stabilization at the interface. This strategy has proved useful for controlling morphology in polyamide blends with ABS[7–9] and SAN copolymers[6,7]. Examples of such compatibilizing additives which have been previously used include styrene–maleic anhydride (SMA) copolymers[6–9], styrene–acrylonitrile–maleic anhydride (S/AN/MA) terpolymers[17], methyl methacrylate/styrene/maleic anhydride (MMA/S/MA) terpolymers[6] and imidized acrylic polymers[6–9].

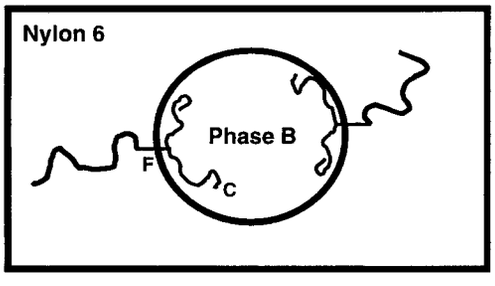

Figure 1 Schematic representation for the optimal location of the graft polymers formed by reaction of the imidized acrylic compatibilizer with nylon 6 in blends with SAN

EXPERIMENTAL

Table 1 lists the pertinent information related to the materials used in this study. The polyamide material used most extensively in this study is a commercially available nylon 6 having molecular weight, $\bar{M}_n = 22\,000$, and contains almost equivalent amounts of carboxyl and amine end groups. The nylon 6,6 material used here has a molecular weight, $\bar{M}_n = 17\,000$. Owing to their hygroscopic character, the polyamides were dried at 80°C in a vacuum oven to remove the sorbed water before processing. The SAN copolymer used in this study is also a commercially available material and has 25 wt% acrylonitrile and will be referred to as SAN 25, or simply SAN, throughout this paper. The imidized acrylic material, IA has 55.7 wt% imide and 2.9 wt% anhydride groups and is miscible with SAN 25[6]. Three different triblock copolymers with styrene endblocks and a hydrogenated midblock were also utilized in this study. The non-reactive triblock copolymer is designated as SEBS while the two maleated versions are designated SEBS-*g*-MA-*X*% where *X* indicates the nominal content of the grafted maleic anhydride (0.46 and 1.84%).

Figure 2 shows the various screw configurations of the 50.8 mm co-rotating Baker Perkins twin screw extruder ($L/D = 10$) used here. The extruder has a clamshell barrel that consists of two halves secured by only two bolts to ensure rapid sampling. Configuration A, which was most extensively investigated in this study contains two sets of kneading sections with the kneaders arranged in a reverse conveying direction at staggering angles of 30°. The first kneading section is located close to the hopper through which the material is fed while the second set of kneaders is located near the extruder exit (see *Figure 2*). Screw sections are located before the first kneading section, between the two kneading sections, and immediately after the second kneading section (all dimensions shown in *Figure 2* are in mm). For all three configurations used in this study the last 51 mm of the extruder has a 'camel screw' element which facilitates forward movement of the extrudate in the final stages of processing. For configuration B the second kneading section is removed, while for configuration C the number of reverse kneaders in the second kneading section is increased from 7 to 11. Configuration D is similar to that of A except that the second set of kneaders is arranged in a neutral configuration with 90° staggering angles.

Screw elements and kneaders used in all three configurations were all 50 mm in diameter. The kneading sections were constructed by arranging standard 2-lobe kneading disks, 12.5 mm thick, at various staggering angles. No die was used at the end of the extruder to avoid complications during the process of opening up the extruder for sample collection. Four different screw speeds of 25, 50, 100 and 200 rpm were used and the temperature of the walls of the extruder was controlled at 240°C, unless otherwise stated. The nylon 6 material was dried at 80°C in a vacuum oven to remove the sorbed water before processing. The extruder was starve fed using a K-Tron feeder at a constant rate of 4.4 kg h^{-1}, unless otherwise stated. Usually a steady state was attained after 20 min of starting the feed. At this point

Table 1 Materials used in this study

Designation used here	Commercial designation	Composition	Molecular weight	Relative melt viscosity[a]	Source
Nylon 6	Capron 8207F	End groups: $NH_2 = 4.4\,\mu eq\,g^{-1}$ $COOH = 43.0\,\mu eq\,g^{-1}$	$\bar{M}_n = 22\,000$	1.0	Allied Signal Inc.
Nylon 6,6	Zytel 101	End groups: $NH_2 = 46.4\,\mu eq\,g^{-1}$ COOH = n.a.	$\bar{M}_n = 17\,000$	1.1[b]	E.I. Du Pont Co.
SAN 25	Tyril 1000	Styrene-acrylonitrile copolymer, 25% AN	$\bar{M}_n = 77\,000$ $\bar{M}_w = 152\,000$	1.0	Dow Chemical Co.
IA[c]	None	Imidized acrylic polymer 55.7 wt% Imide 2.2 wt% free acid 2.9 wt% anhydride	$\bar{M}_w \sim 95\,000$	1.7	Rohm and Haas Co.
SEBS	Kraton G 1652	29 wt% styrene	Styrene Block = 7000 EB Block = 37 500	1.6	Shell Chemical Co.
SEBS-*g*-MA-0.5%	RP-6510	29 wt% styrene 0.46 wt% MA[d]	n.a.	1.5	Shell Chemical Co.
SEBS-*g*-MA-2%	Kraton FG-1901X	29 wt% styrene 1.84 wt% MA[d]	n.a.	1.0	Shell Chemical Co.

[a] Brabender torque at 240°C and 60 rpm after 10 min divided by that of nylon 6
[b] Same as [a] except at 280°C
[c] Miscible with SAN 25
[d] Determined by elemental analysis after solvent/nonsolvent purification
n.a., not available

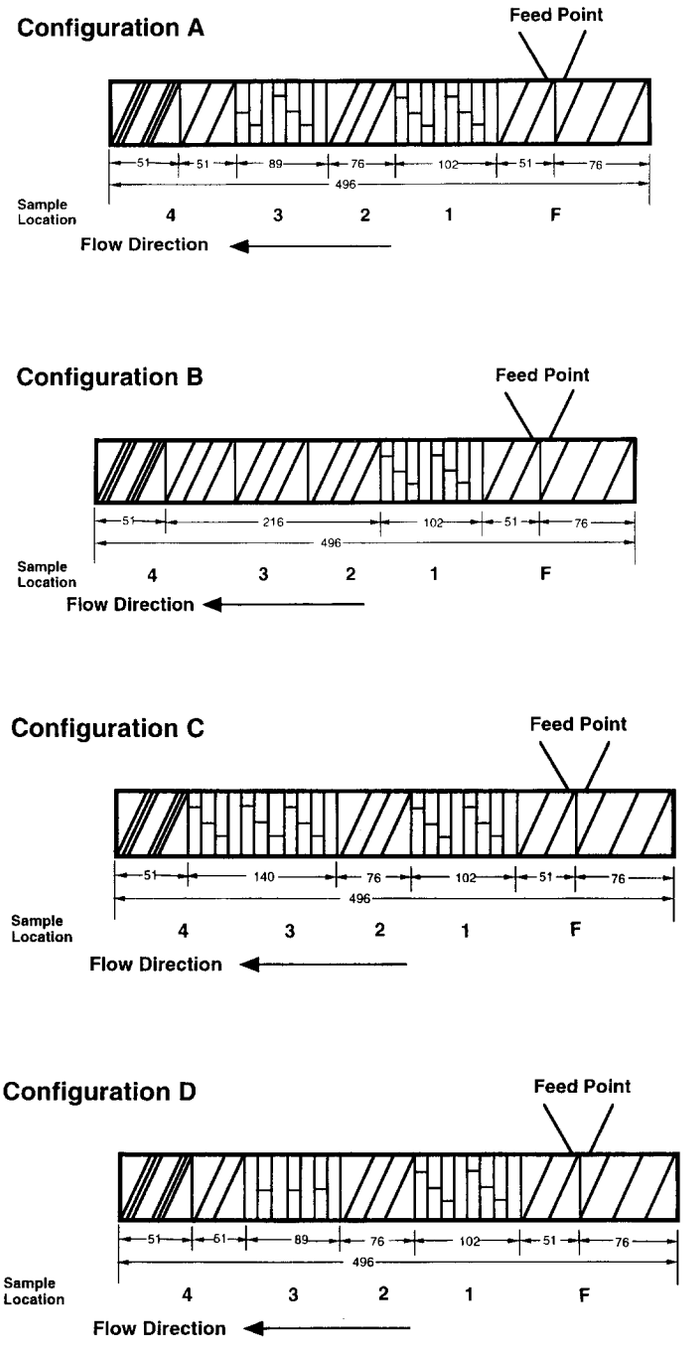

Figure 2 Four different extruder configurations used in this study

the drive was stopped and the extruder opened up by removal of the two bolts. Samples were taken along the length of the extruder at four different locations (see *Figure 2*) and quenched in liquid nitrogen. A maximum of 10 s elapsed between stopping the extruder and quenching the samples. The effect of annealing on the blends was studied by placing the samples extracted from the extruder screw between glass slides on a hot stage at 240°C for 30 min under inert nitrogen purge and then rapidly (<1 s) quenching in liquid nitrogen.

For rheological characterization, the various polymers were tested in a Brabender Plasticorder with a 50 ml mixing head and standard rotors by recording the torque at 240°C and 60 rpm. A Gottfert Rheograph 2001 capillary rheometer ($L/D = 10$) was used to obtain the melt viscosity over a range of shear rates (10–10 000) at 240°C.

The acid and amine end group concentrations for the nylon 6 material and the blends were determined using titration techniques described in detail previously[63]. The acid concentration was analysed by dissolving the polyamide in benzyl alcohol at 110°C and titrating the hot solution to a phenolphthalein end point with 0.01 N KOH/benzyl alcohol. The amine concentration was determined by potentiometric titration, first by dissolving the polyamide in a 15/85 methanol/phenol solution for 48 h and determining the pH inflection while adding a 0.01 N perchloric acid/phenol solution. Blends of nylon 6 were analysed for residual amine concentration as a means of determining extent of reaction, assuming the dominant reaction is between amine and anhydride units to form imide linkages.

Thin sections were cryogenically microtomed using a Reichert–Jung ultramicrotome from samples collected at the four different locations along the screw and stained with either a 2% solution of phosphotungstic acid (to stain the polyamide) or 2% ruthenium tetroxide solution (to stain the SAN) for examination by JEOL 1210 TEM operated at an accelerating voltage of 120 kV. Scanning electron microscopic (SEM) analysis was also employed selectively to view larger particles in uncompatibilized blends using a JEOL JSM-35C SEM operated at 5 kV. These samples were prepared by freezing in liquid nitrogen for 4–5 min and fracturing. A semiautomatic digital image analysis technique was used for determining the dispersed phase domain size from TEM and SEM photomicrographs using NIH Image software. For nonspherical shapes, the diameter was assigned as the average of the major and minor dimensions of each particle. Apparent weight average particle diameters were calculated from measurements on more than 100 particles.

RHEOLOGY

Brabender torque rheometry was utilized to characterize the melt flow behaviour of the individual component polymers used in this study (see *Table 1*). After an initial transient period, all the pure components reached a constant torque value. The value reported here after 10 min of mixing has been used as a means of characterizing these materials. The viscosity ratio between the major phases in the blends reported in this study has been maintained as near as possible to unity to eliminate effects of viscosity mismatch on the final morphology. In some selected cases the results obtained through Brabender rheometry were also corroborated through viscosity vs shear rate measurements generated via capillary rheometry. For example, *Figure 3a* shows viscosity responses of nylon 6 and SAN as a function of shear rate measured using capillary rheometry. While the SAN appears to be slightly more shear-thinning at higher shear rates, at the shear rates expected to prevail in the twin screw extruder ($\sim$100–200 s^{-1}) the two materials are expected to have similar viscosities. Also, this is in accordance with the Brabender torque data shown in *Table 1* where these two components are shown to have similar viscosities. As reported in an earlier study, blends of nylon 6 and the imidized acrylic polymers show a dramatic increase in the overall melt viscosity at certain compositions due to grafting reactions[6].

Figure 3b shows viscosity vs the shear rate plots for the nylon 6 and two styrenic triblock copolymers used in this study as measured by capillary rheometry. These results essentially confirm the observations from Brabender rheometry; the melt viscosity decreases with increasing maleic anhydride content (see *Table 1*) suggesting that some chain scission occurs during the maleation process. Previous studies have demonstrated that blends of polyamide and maleated versions of the styrenic triblock copolymers show significant increase in the viscosity above the additive line due to strong grafting reactions between the nylon 6 and maleic anhydride functionalities[12].

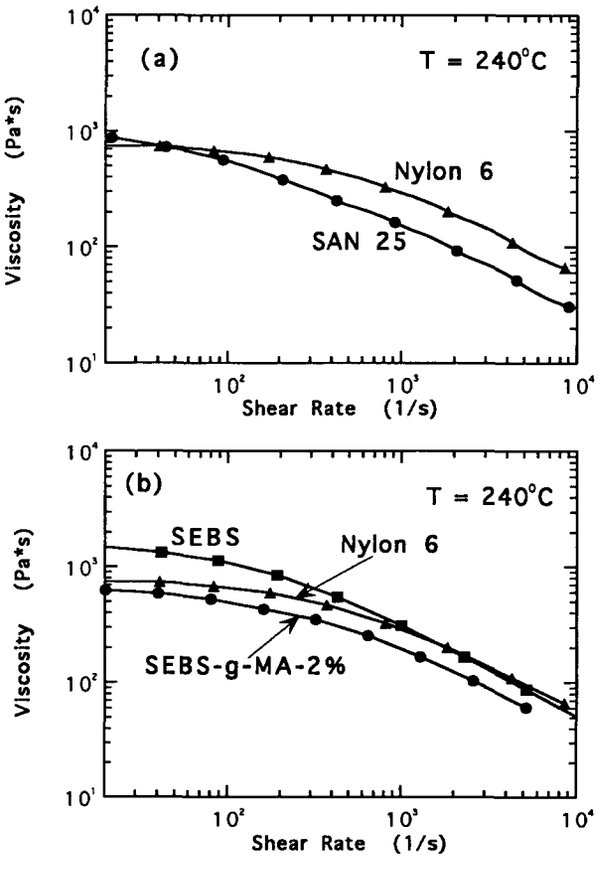

Figure 3 Melt viscosity vs shear rate for (a) nylon 6 and SAN 25; (b) nylon 6, SEBS and SEBS-*g*-MA-2%

MORPHOLOGY GENERATION IN CLAMSHELL EXTRUDER

For all the blends investigated in this study an effort was made to quench samples in liquid nitrogen from various locations in the extruder as quickly as possible to capture the actual morphology of blends in the melt state. In most cases, this was achieved within 8–10 s after stopping the extruder screw. At flow rates investigated in this study the twin screw extruder operates partially starved. This was evident for all the blends investigated here since on opening the clamshell the screw regions were observed to be partially filled with the polymers; while the kneading sections appeared to be nearly flooded.

Uncompatibilized nylon 6/SAN blends

Four different screw speeds (25, 50, 100 and 200 rpm) were used to study the development of morphology along the extruder using configuration A for the binary nylon 6/SAN (75/25) blends. *Figure 4* shows a representative series of SEM photomicrographs of samples collected from four different locations along the screw at 100 rpm using extruder configuration A. In general, for all four screw speeds utilized in this study the particle size of the dispersed SAN phase decreases along the length of the screw and efficiency of dispersion is favoured by an increase in the screw speed. In this series, SEM analysis was preferred to TEM as it provided a wider field of view of the dispersed phase particles which were mostly >1 μm in size. TEM analysis was performed selectively on a few blends in this series as shown in *Figure 5*. The dimensions of the dispersed phase as revealed in TEM photomicrographs are in reasonable agreement with that observed using SEM analysis. In addition, TEM analysis

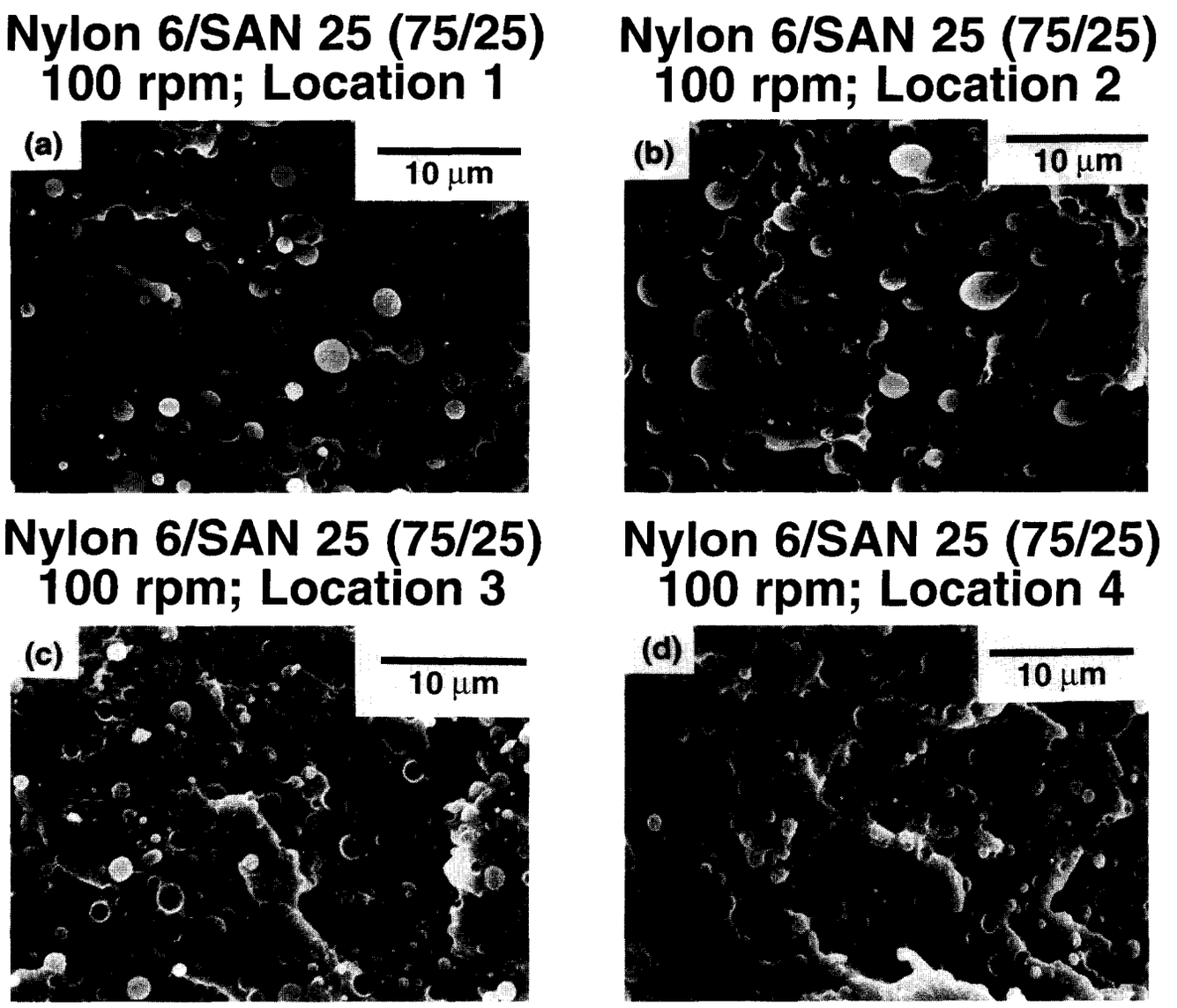

Figure 4 SEM photomicrograph of nylon 6/SAN 25 (75/25) blend samples collected from four locations in the clamshell extruder (see *Figure 2*) at a screw speed of 100 rpm with extruder configuration A

of samples extracted from the initial regions of the screw (locations 1 and 2) revealed occlusions of polyamide within the dispersed SAN phase as shown in *Figure 5a* which are not detectable through SEM techniques.

Figure 6 shows the variation of particle size of the SAN dispersed phase along the length of the extruder at four different screw speeds estimated from SEM photomicrographs. Between 25 and 100 rpm, increasing the screw speed leads to a steady decrease in the dispersed phase particle size at all four locations along the screw; but, increasing screw speed to 200 rpm shows some departure from this dependency. For 200 rpm, although the particle size in the initial regions of the extruder (locations 1 and 2) is smaller than the corresponding values for 100 rpm, locations 3 and 4 show a somewhat larger particle size.

Compatibilized nylon 6/SAN blends

For the compatibilized blends, SEM techniques were not useful as the dispersed phase particle size was below the limits of resolution of this technique even in the initial regions of the extruder. Hence, TEM techniques were mainly used for quantifying the dispersed phase particle size of these blends. The particle size in these blends was investigated as a function of extruder screw speed and configuration, compatibilizer content, concentration of the dispersed phase and flow rate.

Effects of varying screw speed. The effects of varying screw speed on the morphology of compatibilized blends was investigated using mostly configuration A of the clamshell extruder (see *Figure 2*). *Figure 7* shows TEM photomicrographs of nylon 6/SAN blends compatibilized with 5% imidized acrylic polymer, IA, at four different locations along the screw at 100 rpm screw speed. The blend exhibits a dramatic decrease in particle size at location 1 almost immediately after melting in the initial stages of the first kneading section (*Figure 7a*). Most of the particles appear to be below 0.2 μm in size along with a distinct population of larger particles ($\sim$0.5 μm). In contrast, the dispersed phase particles at location 2 are significantly more monodisperse with average particle size $\sim$0.15 μm. At location 3 there is a pronounced shift in this distribution with the emergence of two distinct populations of particles – the smaller being in the 0.05–0.2 μm range and the larger in the 0.3–0.4 μm

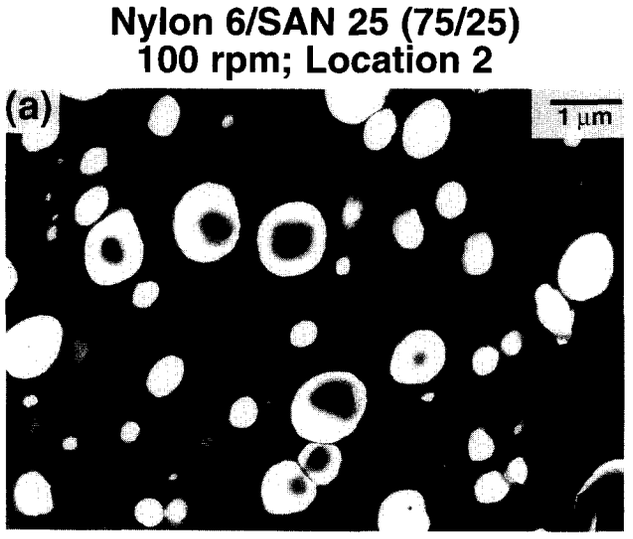

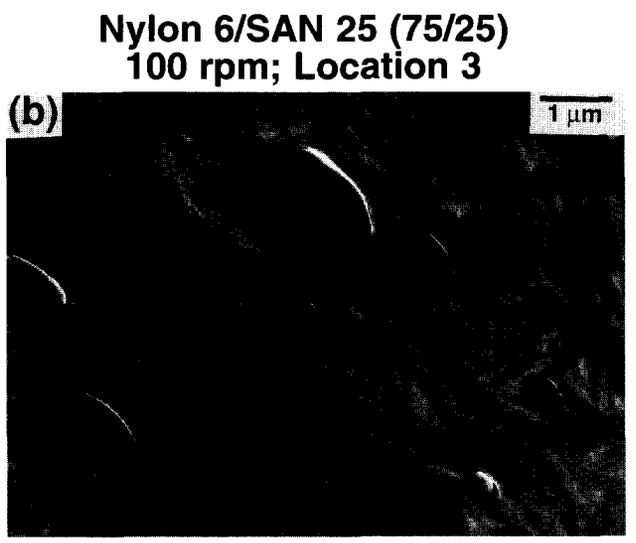

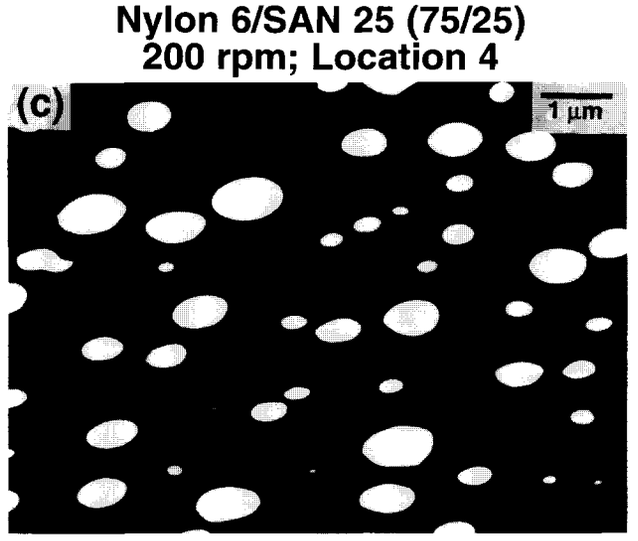

Figure 5 TEM photomicrographs of nylon 6/SAN 25 (75/25) blend samples collected from (a) location 2 where phosphotungstic acid (PTA) has been used as a staining agent; (b) location 3 where RuO_4 has been used as a staining agent at a screw speed of 100 rpm; and (c) location 4 at a screw speed of 200 rpm where PTA has been used as staining agent

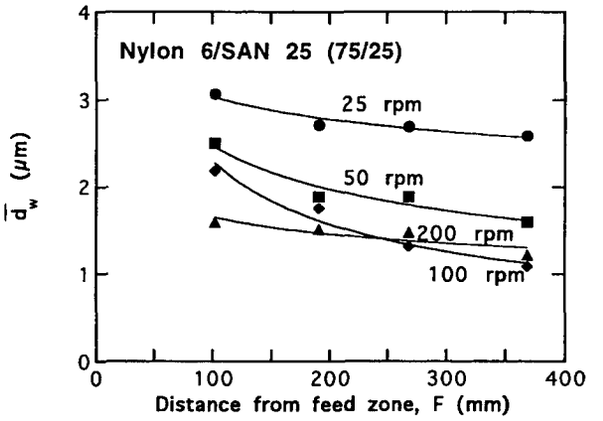

Figure 6 Dispersed phase particle size as a function of the distance from the feed zone of the clamshell extruder for nylon 6/SAN 25 blends at 25, 50, 100 and 200 rpm screw speed. The average particle size $\bar{d}_w$ has been computed from SEM photomicrographs

range. This duality in particle size becomes even more distinct at location 4 where the larger population of particles has increased in size (0.3–0.6 μm). *Figure 8* shows TEM photomicrographs for locations 2 and 4 for nylon 6/SAN/IA blends at similar composition at 50 and 200 rpm which display trends similar to that observed earlier where a distinct population of particles with significantly larger size is observed after the second kneading section. *Figure 9* shows selected histogram plots for particle size distribution at different locations in the extruder for nylon 6/SAN/IA blends for three different screw speeds used in this work. The significant broadening of the distribution of particle size towards the end of the second kneading section is evident for all three screw speeds shown here.

Figure 10 compares the dispersed phase particle size in nylon 6/SAN/IA (75/20/5) blends at three different screw speeds. While the dispersed phase particle size shows an apparent minimum at location 2 for screw speeds of 100 and 200 rpm; it displays a minimum particle size between locations 2 and 3 when the screw speed is 50 rpm. Also, the dispersed phase particle size at location 4 is significantly larger at the highest screw speed, i.e. 200 rpm. *Figure 11* provides a comparison of the morphology generation along the screw in uncompatibilized vs compatibilized nylon 6/SAN blends. It is clear that there is an order of magnitude difference in the particle size between these two cases at all four locations along the screw at all screw speeds used.

Effect of varying screw configuration. Figure 12 shows a series of TEM photomicrographs of nylon 6/SAN/IA blends at location 4 for different screw configurations employed in this study. For screw configuration B in which the second set of reverse kneading blocks is eliminated, the dispersed phase particle size at location 4 is significantly smaller than that observed previously for configuration A (see *Figure 12a*). On the other hand, increasing the number of reverse kneading disks in the second kneading section (configuration C) leads to a significant increase in the dispersed phase particle size at 100 rpm (*Figure 12b*). *Figure 12c* shows the effects of changing the configuration of the second set of kneading blocks from reverse to neutral. The dispersed phase particle size for this configuration is significantly smaller

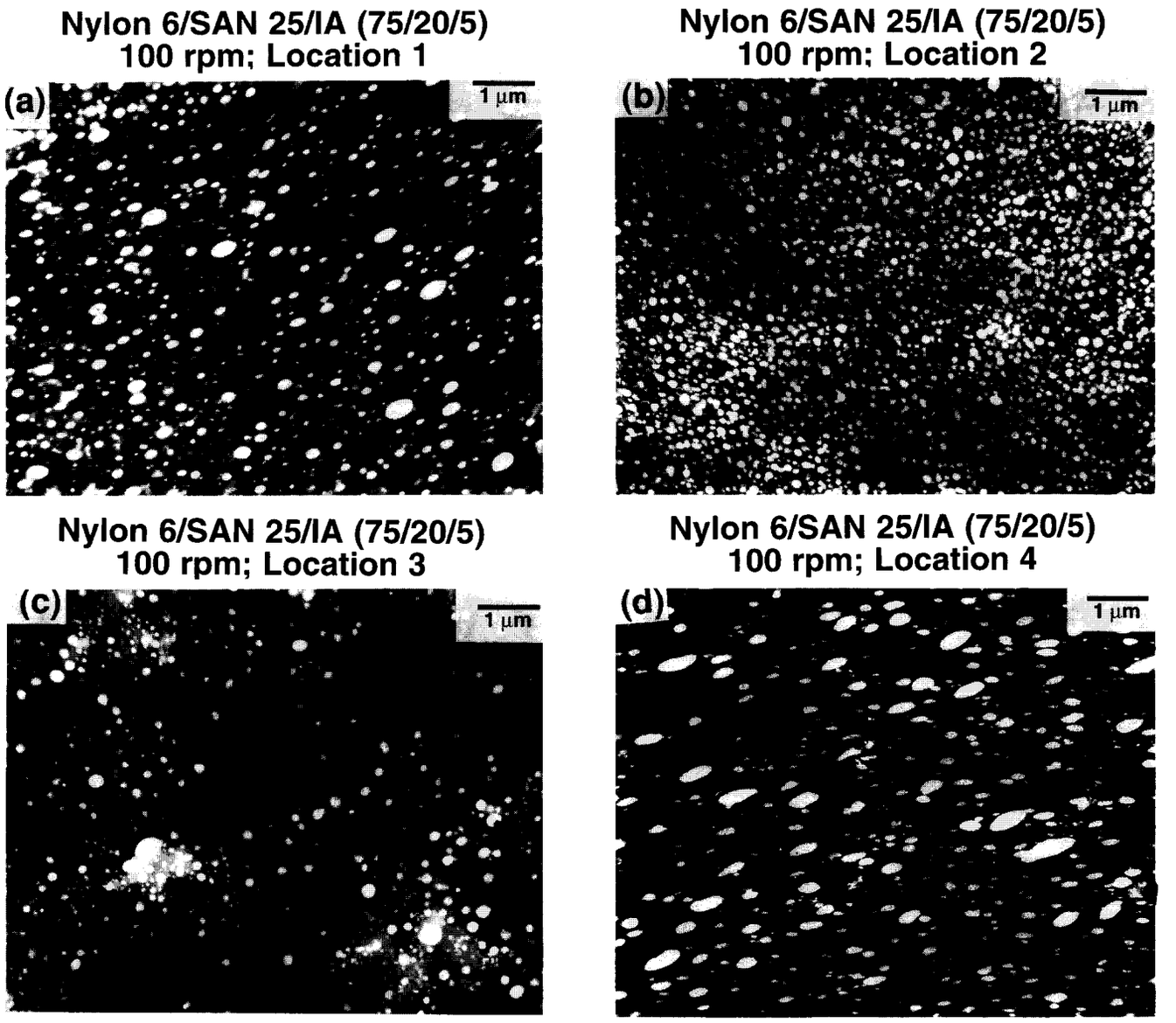

Figure 7 TEM photomicrographs of nylon 6/SAN 25/IA (75/20/5) blend samples taken from (a) location 1; (b) location 2; (c) location 3; and (d) location 4 of the clamshell extruder operating at 100 rpm with extruder configuration A

than that observed at location 4 for configuration A and is comparable to dispersed phase particle size observed for configuration B. Limited experiments done at a higher screw speed of 200 rpm for configuration C revealed a much larger particle size (see *Figure 12d*) than that obtained at 100 rpm.

Figure 13 shows the particle size distribution at location 4 for configurations B and C at 100 rpm. As expected, configuration B yields a significantly narrower particle size distribution than configuration C. The particle size distribution for configuration D (not shown here) is very similar to that obtained for configuration B. *Figure 14* illustrates this issue further by showing the average particle size *versus* the screw length for four different screw configurations used in this study at 100 rpm. It is clear from the TEM photomicrographs in *Figure 12* that for configurations B and D there is little difference between the dispersed phase particle size at locations 2 and 4, while for configuration C there is a dramatic increase in the dispersed phase particle size between these two locations.

Effects of changing compatibilizer content, flow rate and composition. *Figure 15* shows TEM photomicrographs at four different locations for nylon 6/SAN/IA blends prepared at 100 rpm with extruder configuration A in which the concentration of the IA compatibilizer is increased to 8%. Although the average particle size at all locations in the extruder is lower than that for the corresponding blend with 5% compatibilizer, the overall trend in the evolution of morphology parallels the observations made earlier. Similar to trends observed previously there is evidence of significant coalescence at locations 3 and 4 where a distinct population of particles 0.4–0.6 μm in size co-exist with much smaller particles (0.05–0.2 μm). Increasing the screw speed to 200 rpm leads to an even greater degree of phase coarsening than that observed for the corresponding blend at 5% compatibilizer concentration as shown in the TEM photomicrograph in *Figure 16*.

Limited experiments were carried out with lower concentrations of the dispersed phase (maintaining

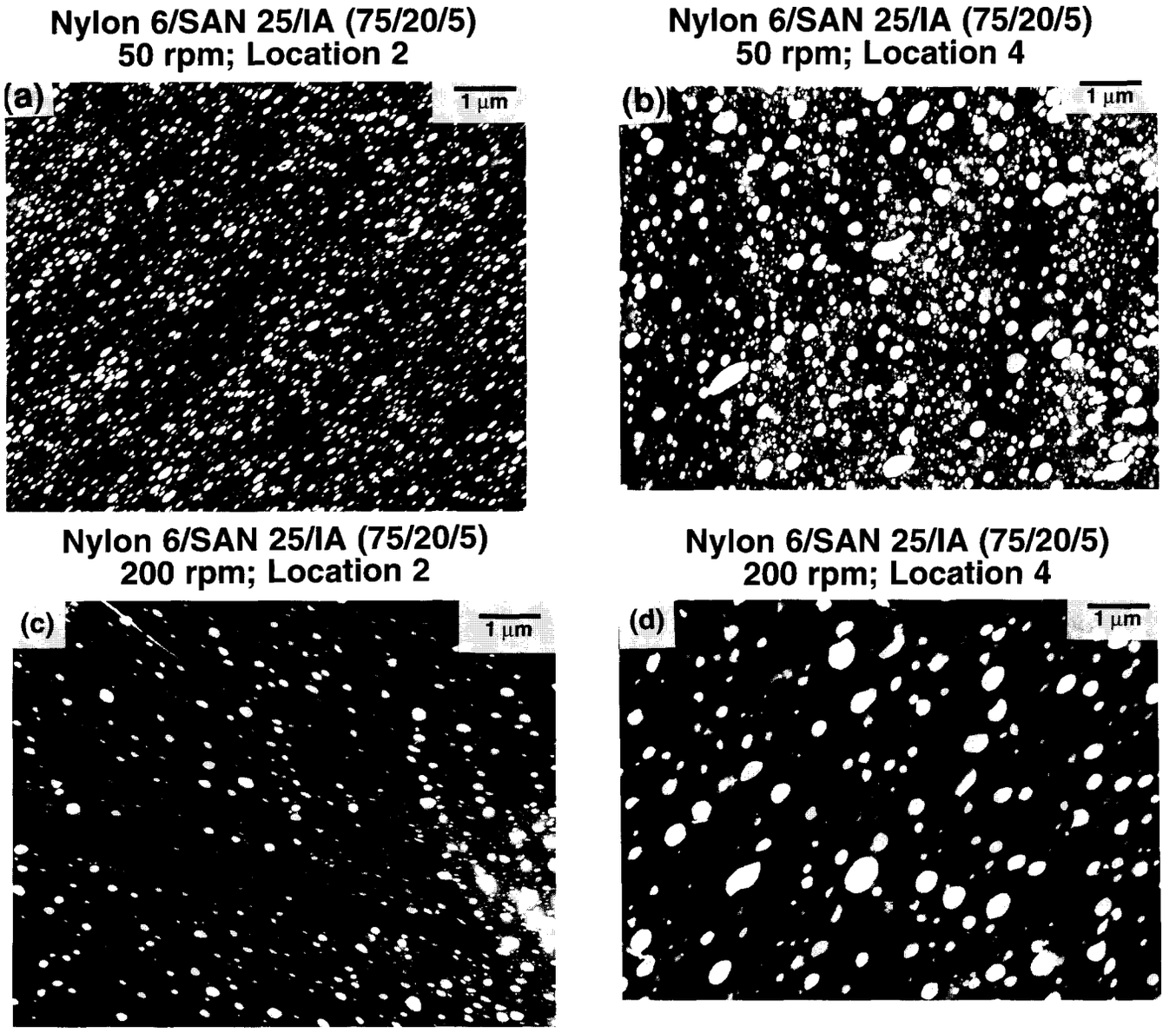

Figure 8 TEM photomicrographs of nylon 6/SAN 25/IA (75/20/5) blend samples taken from locations 2 and 4 at 50 rpm ((a) and (b)) and 200 rpm ((c) and (d)) with extruder configuration A. The polyamide phase has been stained with phosphotungstic acid

identical SAN 25/IA ratio) to test the hypothesis that reducing the fraction of the minor phase will diminish the extent of coalescence[42]. *Figure 17* shows TEM photomicrographs for nylon 6/SAN/IA (85/12/3) blend at locations 2 and 4 (for configuration A) along the screw at 100 rpm. Practically no difference can be detected either in dispersed phase particle size or its distribution between these two TEM photomicrographs which clearly demonstrates a significantly reduced contribution from coalescence mechanisms at lower minor phase concentrations in reactively compatibilized nylon 6/SAN blends.

Figure 18 shows TEM photomicrographs for locations 2 and 4 when the flow rate is increased to $6.7\,kg\,h^{-1}$ using extruder configuration A. Although the dispersed phase particle size is somewhat larger at location 2 than what was observed previously for the lower flow rate (see *Figure 7b*), there is still some evidence of coalescence at this higher flow rate at location 4 where a dual population of particles is observed (*Figure 18b*).

Effects of annealing. Limited annealing experiments were carried out to test stability of the dispersed phase morphology at various locations in both the uncompatibilized and compatibilized blends in the melt state at 240°C under inert nitrogen for 30 min. No significant change in the blend morphology was observed after annealing in either the uncompatibilized or compatibilized blends. *Figure 19* shows photomicrographs at positions 2 and 4 for nylon 6/SAN 25/IA blends at locations 2 and 4 which have almost identical average dispersed phase particle size and size distribution as the unannealed blends (see *Figures 7b* and *7d*). Similar results were obtained for all blends which were analysed after annealing under quiescent conditions.

Extent of reaction

Figure 20 compares the extent of reaction and dispersed phase particle size along the screw for configuration A at three different screw speeds. For the lowest screw speed, 50 rpm, the reaction proceeds least

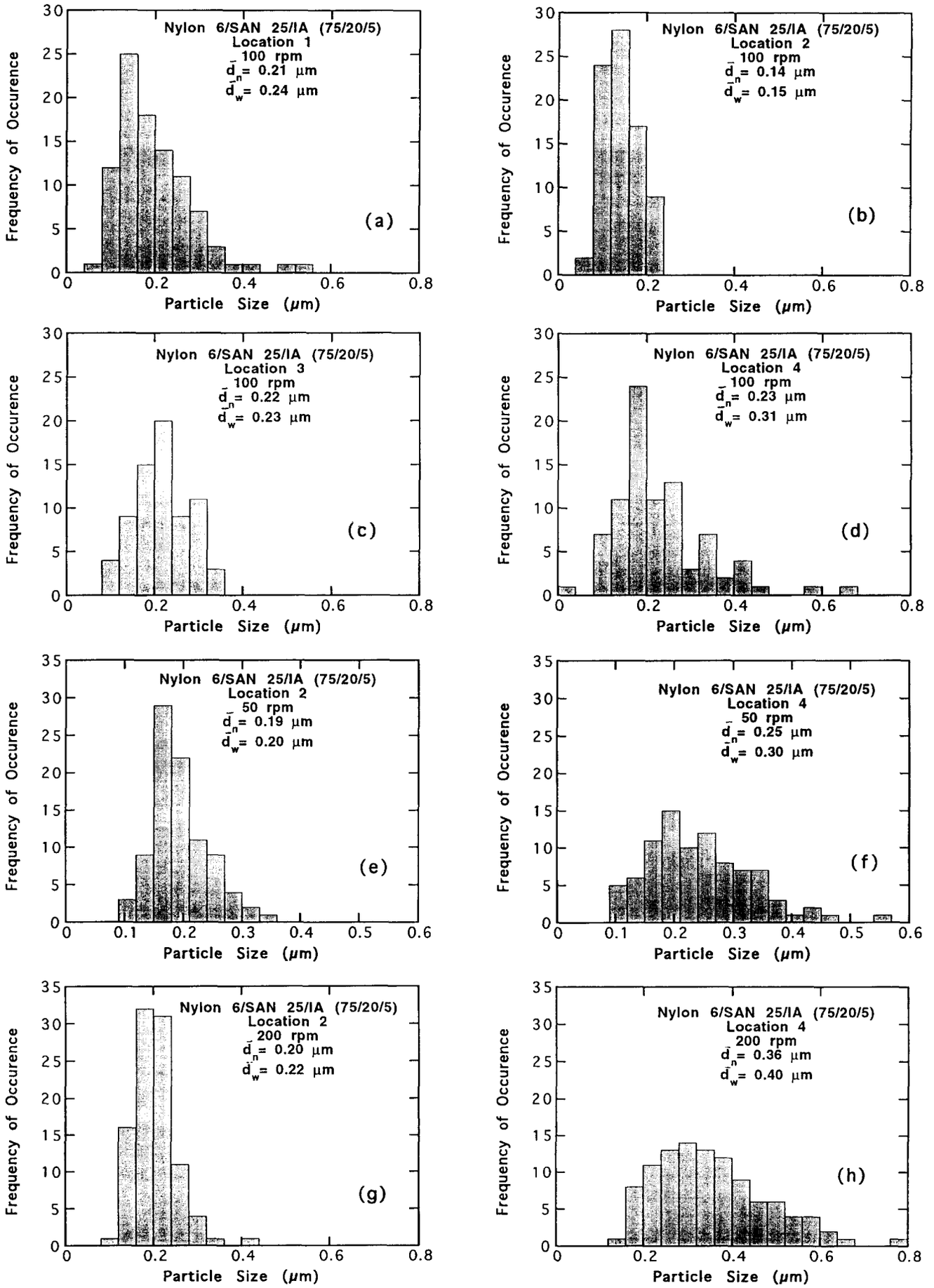

Figure 9 Particle size distribution of nylon 6/SAN 25/IA (75/20/5) blends calculated from TEM photomicrographs in *Figures 7* and *8* at different locations in the extruder at 50, 100 and 200 rpm

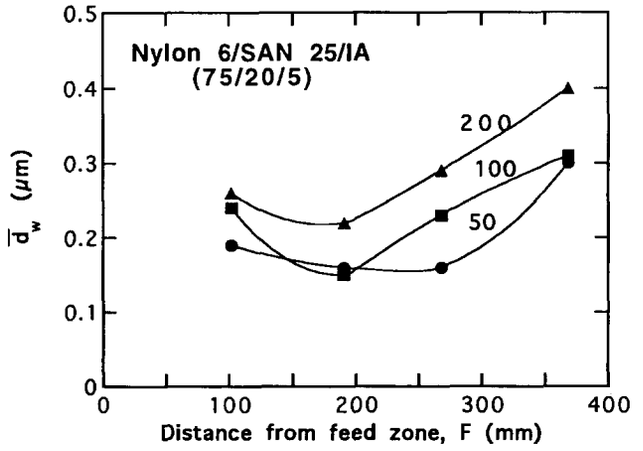

Figure 10 Dispersed phase particle size as a function of distance from the feeding zone of the clamshell extruder for nylon 6/SAN 25/IA (75/20/5) blends at 50, 100 and 200 rpm screw speed. The average particle size, $\bar{d}_w$, has been computed from TEM photomicrographs shown in *Figures 7* and *8*

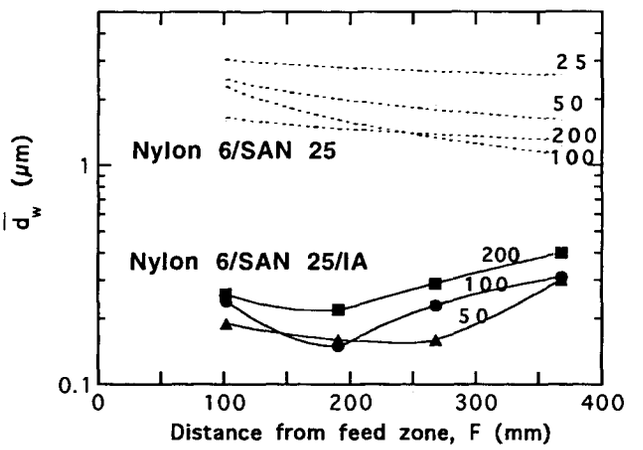

Figure 11 Comparison of dispersed phase particle size as a function of the distance from the feeding zone of the clamshell extruder for uncompatibilized vs compatibilized blends at various screw speeds

rapidly with almost a linear increase in the fraction of the amine groups consumed along the screw. On the other hand, for 200 rpm, the reaction reaches its maximum limit in the initial regions of the screw. From *Figure 20* it appears that screw speed, extent of reaction and dispersed phase particle size along the screw are all inter-related. In all three cases coalescence appears to become dominant only after most of the functional groups have been consumed. It is also clear that only a small amount (<20%) of reaction is necessary to lower the particle size to its minimum level (see *Figure 20a* for 50 rpm).

Table 2 lists the dispersed phase particle size and extent of reaction at location 4 for the four different screw configurations used in this study at 100 rpm. Extruder configurations that involve more intensive mixing (A and C) in the latter stages of the screw show significantly higher extents of reaction (~45%) than configurations that utilize less intensive mixing in the latter stages of the screw (B and D). Increasing the flow rate also leads to diminished extent of reaction at all screw locations sampled (see *Table 2*).

Table 2 Extent of reaction and dispersed phase particle size for selected nylon 6/SAN 25/IA (75/20/5) blends at 100 rpm screw speed

Extruder configuration	Flow rate ($kg\,h^{-1}$)	$\bar{d}_w$ at location 4	Extent of reaction, x, at location 4
A	4.4	0.31	0.45
B	4.4	0.16	0.30
C	4.4	0.37	0.46
D	4.4	0.20	0.30
A	6.7	0.29	0.37

POLYAMIDE/SEBS BLENDS

Limited experiments were conducted with nylon 6 and nylon 6,6 blends with the elastomeric triblock copolymers SEBS, SEBS-*g*-MA-2% and SEBS-*g*-MA-0.5% to compare evolution of morphology along the screw to observations made with the nylon 6/SAN blends. All the results reported here utilize extruder configuration A and a screw speed of 100 rpm.

Nylon 6/SEBS

Figure 21 shows SEM photomicrographs for nylon 6/SEBS blends taken from various locations in the clamshell extruder at 100 rpm. This blend shows significantly slower reduction in particle size compared to the uncompatibilized nylon 6/SAN blend described previously. Both fibrillar and spherical structures are observed to co-exist at locations 1 and 3 along the extruder; while predominantly spherical structures are observed at location 4 (near the exit of the extruder). The second kneading section in the extruder undoubtedly contributes to increasing the efficiency of mixing in this case.

Nylon 6 and nylon 6,6 blends with SEBS-g-MA-2%

Figure 22 shows TEM photomicrographs for blends of nylon 6 and nylon 6,6 with SEBS-*g*-MA-2% at locations 1 and 4 along the extruder screw (see configuration A in *Figure 2*). While the dispersed phase particles for the nylon 6/SEBS-*g*-MA-2% blend are mostly spherical in shape and lower than 0.08 μm in size at all locations along the screw, the dispersed phase particles in the nylon 6,6/SEBS-*g*-MA-2% are somewhat more complex and larger in size (~0.15 μm). Also, for the nylon 6 blend the dispersed phase is uniformly distributed in the polyamide matrix at all locations as opposed to the nylon 6,6 blend where domains of the dispersed rubber phase appear to be aggregated together at location 1 and much more uniformly distributed at location 4. However, from a careful scrutiny of TEM photomicrographs in this series it is clear that even for the nylon 6,6 blend there is little difference in the dimensions of rubber particles along the length of the screw. *Figure 23* illustrates this by plotting the particle size vs length along the screw for these two systems.

Nylon 6/SEBS/SEBS-g-MA-2% vs nylon 6/SEBS-g-MA-0.5% blends

Figure 24 shows comparison of dispersed phase particle size of samples (computed from TEM photomicrographs) collected from different locations in the clamshell extruder for nylon 6/SEBS/SEBS-*g*-MA-2% (80/15/5) and nylon 6/SEBS-*g*-MA-0.5% (80/20) blends which contain almost identical concentration of MA in the dispersed phase. While in both blends there is a

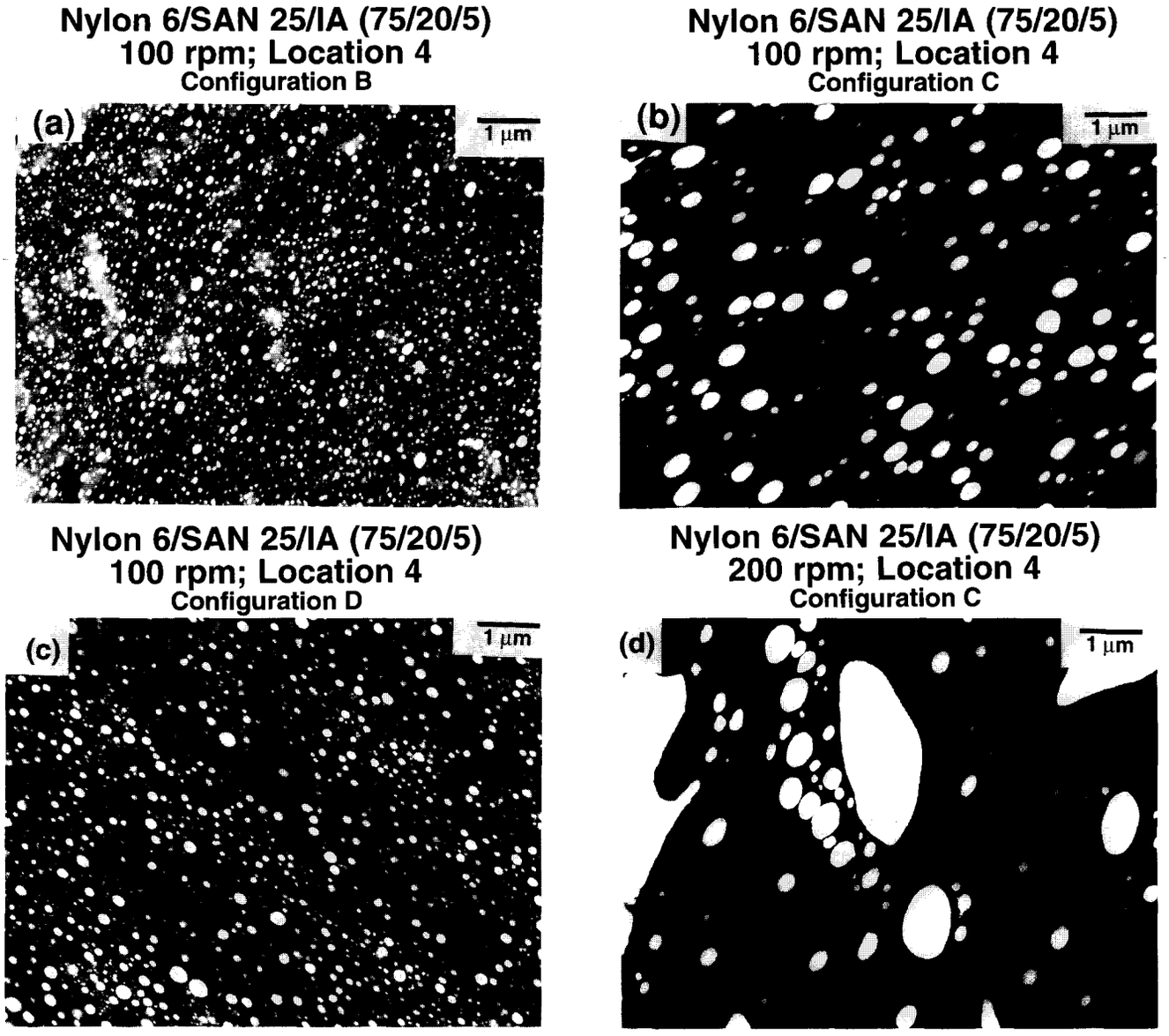

Figure 12 TEM photomicrographs of samples taken from location 4 of nylon 6/SAN 25/IA (75/20/5) blends for extruder configuration (a) B at 100 rpm; (b) C at 100 rpm; (c) D at 100 rpm; and (d) C at 200 rpm. Note distinct dual population of dispersed phase particles for (d) in which the estimated $\bar{d}_w \sim 1\,\mu m$

dramatic drop in the dispersed phase particle size in the initial region of the extruder (locations 1 and 2), the ternary nylon 6/SEBS/SEBS-*g*-MA blend shows an increase in the average particle size at the exit (location 4) by ~100% compared to its average dimensions at location 2.

Extent of reaction

Figure 25 shows the progression of the amine–anhydride reaction as a function of sample location along the screw for the reactively compatibilized nylon 6/SEBS systems investigated in this study. As expected, the nylon 6/SEBS-*g*-MA-2% (80/20) blend shows significantly higher extent of reaction (~65%) than the nylon 6/SEBS-*g*-MA-0.5% (80/20) and nylon 6/SEBS/SEBS-*g*-MA-2% (80/15/5) blends which contain a lower concentration of MA in the dispersed rubber phase. For the blends with a lower concentration of MA (nylon 6/SEBS-*g*-MA-0.5% and nylon 6/SEBS/SEBS-*g*-MA-2%), there is comparable extent of reaction at the exit of the extruder (~30%) but the reaction profiles differ along the screw. While for the binary nylon 6/SEBS-*g*-MA-0.5% (80/20) blend the amine–anhydride reaction progresses continuously along the screw, in the case of the ternary nylon 6/SEBS/SEBS-*g*-MA-2% (80/15/5) blend most of the amine groups are consumed in the initial regions of the screw with very little change downstream along the extruder.

It is worth mentioning that at location 1 the binary nylon 6/SEBS-*g*-MA-2% and the ternary nylon 6/SEBS/SEBS-*g*-MA-2% blends have almost identical extents of reaction which correspond to a majority of the MA groups having reacted in the ternary blend but only a small fraction of the available MA groups in the binary blend[115]. Thus, beyond location 2 there is little change in the extent of reaction for the nylon 6/SEBS/SEBS-*g*-MA-2% blend, while for the nylon 6/SEBS-*g*-MA-2% blend there is a steady increase in the extent of reaction almost until the exit of the extruder where

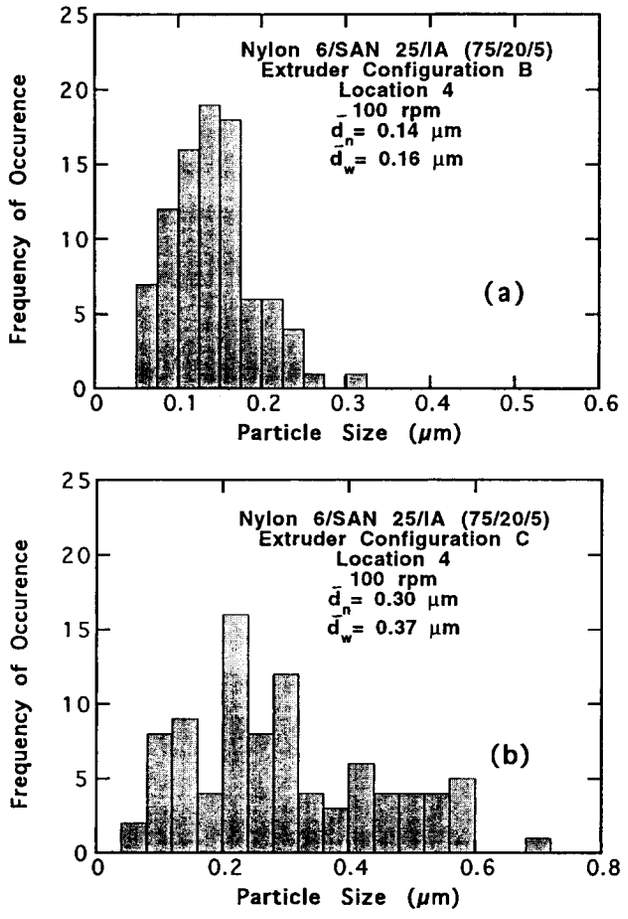

Figure 13 Particle size distribution of nylon 6/SAN 25/IA (75/20/5) blend samples taken from location 4 at 100 rpm screw speed for extruder configurations (a) B and (b) C

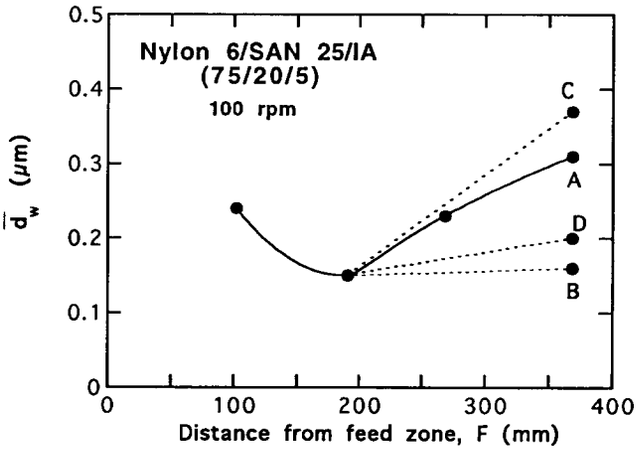

Figure 14 Dispersed phase particle size as a function of the distance from the feed zone of the clamshell extruder for nylon 6/SAN 25/IA (75/20/5) blends at 100 rpm for extruder configurations A, B, C and D

most of the anhydride groups grafted to the SEBS have reacted.

DISCUSSION

For the non-reactive blends investigated in this study the evolution of morphology along the twin screw extruder has been found to be quite similar to that reported by earlier investigators[92–105]. In general, the dispersed phase particle size becomes progressively smaller and less complex along the screw length and with increasing screw speed. In the case of the uncompatibilized nylon 6/SAN blends where this phenomenon was more intensely investigated some coalescence was observed towards the end of the screw at high screw speeds. Such behaviour has been reported in the past by several investigators[56–58], and could be related to several complex and often inter-related issues including higher probability of collision of dispersed phase particles during more intensive mixing, shift in viscoelastic properties of individual components of the blend at higher stress levels and shorter residence time in the extruder. The evolution of morphology for the uncompatibilized nylon/SEBS blend along the screw was observed to be significantly more sequential with fibrillar structures of the dispersed phase in the initial regions of the extruder gradually breaking up into smaller droplets downstream in the extruder. This distinctly slower development of morphology in the polyamide/SEBS blends could be related to the considerably greater elastic character of the SEBS block copolymer as compared to the SAN phase.

For the nylon 6/SAN blends reactively compatibilized with the imidized acrylic polymer a dramatic decrease in the dispersed phase particle size is observed in the very initial stages of the extruder almost immediately after melting of the blended materials. Also, a distinct minimum in particle size for these blends is observed at an intermediate location for all screw speeds (50, 100 and 200 rpm) with extruder configuration A. Lowering the screw speed to 50 rpm, however, appears to postpone the onset of coalescence to a much later zone in the screw. Both the onset and the extent of coalescence appear to depend on a combination of different factors including screw speed, type of mixing elements beyond the melting section in the screw (first kneading section), compatibilizer content, volume fraction of the dispersed phase and flow rate.

Monitoring the extent of reaction along the screw yields interesting insights into the relationship between the chemical reaction at the interface and progression of phase morphology along the extruder screw. In particular, the onset of coalescence along the screw appears to be related to the reaction profile along the extruder. Higher screw speeds lead to more rapid melting and mixing of the blended materials and a more rapid consumption of the functional groups in the initial region of the screw which could promote an earlier onset of coalescence. The final extent of reaction of the blends for a fixed composition at the exit of the extruder is dependent on the screw speed, screw configuration and flow rate. In general, coalescence appears to become prominent in the ternary nylon 6/SAN/IA reactive blends after most of the functional groups have been consumed. For a fixed flow rate and composition it is possible to delay the onset of coalescence by either lowering the screw speed or introducing less intensive mixing elements in the latter stages of the screw. In both situations the chemical reaction between the polyamide chains and the imidized acrylic polymer is slowed down to a significant degree.

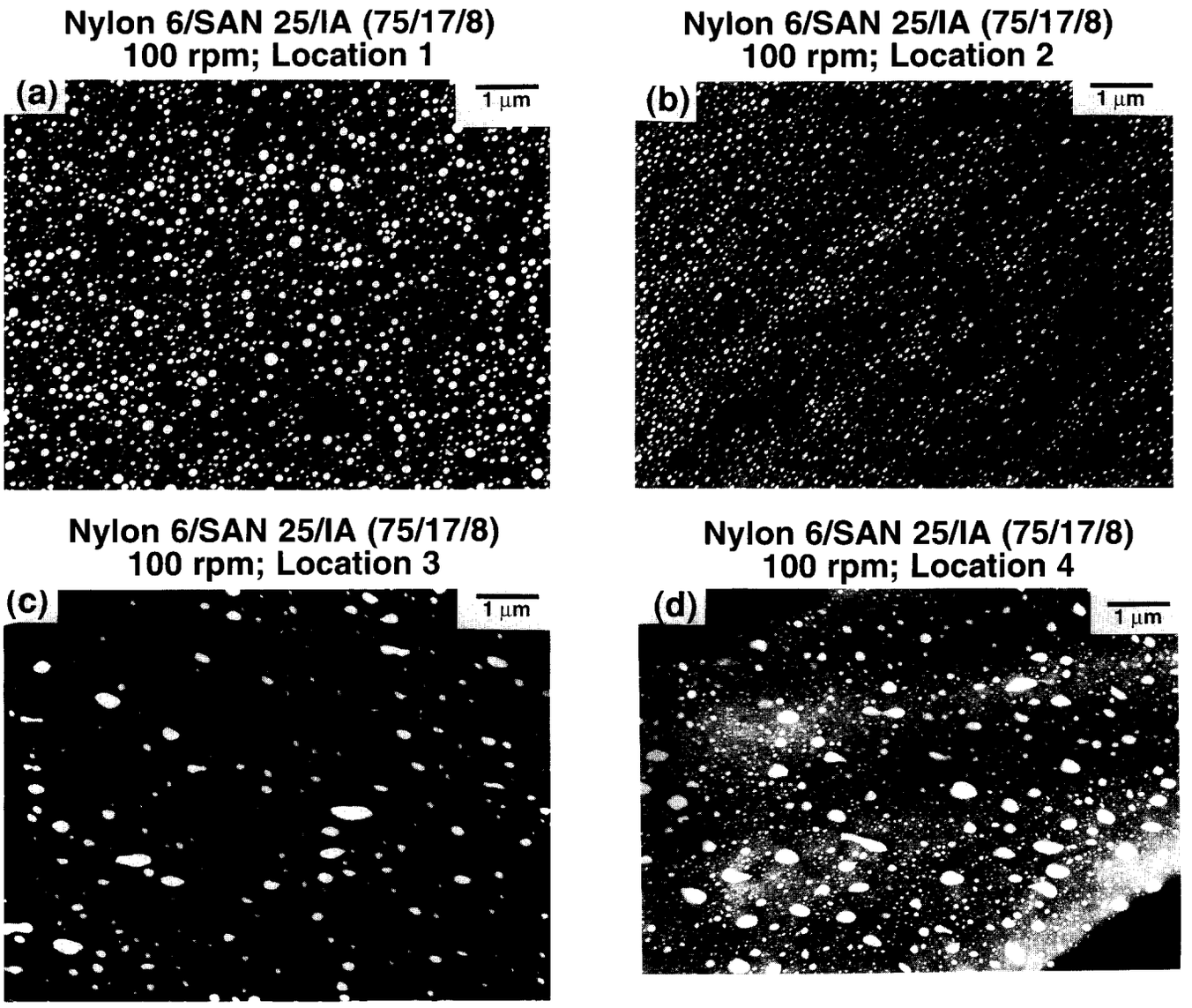

Figure 15 TEM photomicrographs of nylon 6/SAN 25/IA (75/17/8) blend samples taken from (a) location 1; (b) location 2; (c) location 3; and (d) location 4 of the clamshell extruder operating at 100 rpm. The dispersed phase particle size is at its minimum at location 2, $\bar{d}_w = 0.17\,\mu m$ and maximum at location 4, $\bar{d}_w = 0.28\,\mu m$. Note the distinct dual population of particles at location 4

For the reactive nylon 6/SAN blends investigated here, the functional groups in the imidized acrylic polymer appear to limit the maximum extent of reaction that is possible. For compositions reported here, the maximum extent of reaction of the amine groups in the nylon 6 material is ~45%. This corresponds to almost total reaction with anhydride groups in the imidized acrylic polymer along with a significant fraction of the free acid groups (some of which may be converted to anhydride during the blending process, see refs 6 and 15) and should be sufficient for providing adequate steric stabilization against coalescence of the dispersed phase particles. In that case, what is the mechanism behind the coalescence phenomenon in the latter stages of extrusion in the reactive blends? Based on the evidence presented here we propose the following explanation. The imidized acrylic polymer chemically reacts with the polyamide phase but is only physically held in the SAN phase. High stresses may remove the imidized acrylic backbone of the graft copolymer from the SAN phase. This becomes an even greater possibility if the molecular composition of the imidized acrylic compatibilizer is altered through chemical reactions with amine end groups in the polyamide to an extent that it ultimately becomes immiscible with the SAN phase. If the graft copolymer is removed from the nylon 6/SAN interface under the high rheological stresses that exist in the kneading sections of the extruder, this would leave the dispersed phase surface with a significantly depleted coverage, making it more susceptible to coalescence. It can also be speculated that the distinct population of particles with extremely small particle size observed in samples collected from locations near the exit of the extruder correspond to micellar aggregates of the imidized acrylic polymer which have phase-segregated from the interface.

The observations with binary blends of SEBS-*g*-MA-2% with nylon 6 and nylon 6,6 clearly indicate that the topology of grafting of the polyamide chains can play a pivotal role in creating differences in morphology generation along the twin screw extruder in reactive blends. The one point attachment of the monofunctional nylon 6 material leads to a more efficient formation

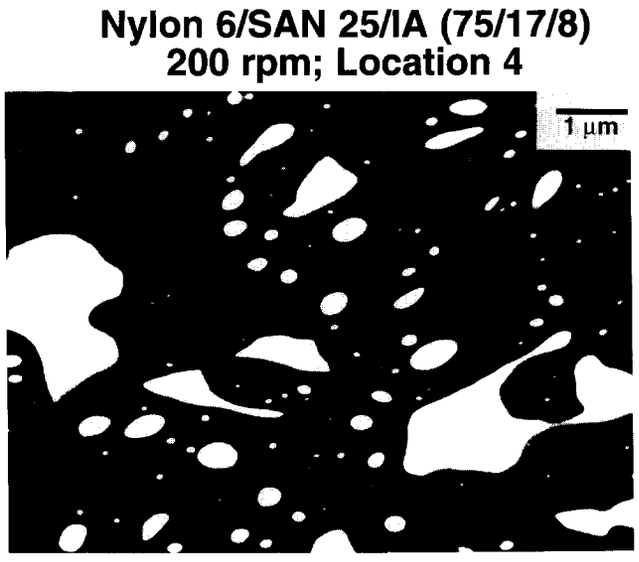

Figure 16 TEM photomicrograph of nylon 6/SAN 25/IA (75/17/8) blend taken from location 4 of the clamshell extruder operating at 200 rpm and extruder configuration A. Large irregular (2–4 μm) shaped particles are observed to co-exist with much smaller ones (~0.15 μm). The average particle size for this blend, $\bar{d}_w = 0.55\,\mu$m

of small spherical particles (~0.05–0.08 μm) almost immediately after melting of the pellets at location 1 in the twin screw extruder. These particles are apparently sterically stabilized to an adequate extent in that the particle shape and size remain unchanged even after the blend passes through the second kneading section. It is possible that this is a consequence of chemical reaction occurring continuously along the extruder screw leading to a significantly higher fraction of amine end groups (~65%) that ultimately react with the MA groups attached to the SEBS-*g*-MA-2%. Also, since the maleic anhydride groups are now bound chemically to both the SEBS and the polyamide chains it is much more difficult to mechanically rip these away from the interface. The difunctional nylon 6,6 on the other hand, yields particles which are significantly larger in size (~0.15 μm) and aggregated together in the initial regions of the extruder. This is no doubt related to the fact that a certain fraction of the chains in nylon 6,6 have two amine end groups and are, thus, difunctional with respect to the anhydride reactive groups attached to the SEBS, which could lead to the formation of loops or bridges, i.e. 'crosslinking' effects, to generate more complex distribution of the dispersed phase particles[9,12,13]. The second kneading section in the extruder appears to facilitate more efficient distributive mixing without changing significantly the dimensions of the individual dispersed phase particles.

Although both the nylon 6/SEBS/SEBS-*g*-MA-2% and the nylon 6/SEBS-*g*-MA-0.5% blends contain similar concentrations of MA groups in the elastomeric phase, both the morphology and the reaction profile evolve very differently along the extruder screw. While a minimum dispersed phase particle size is attained in both cases at location 2, there is pronounced coalescence observed in case of the ternary nylon 6/SEBS/SEBS-*g*-MA-2% (80/15/5) blend as opposed to practically no change in the average particle size for the binary nylon 6/SEBS-*g*-MA-0.5% (80/20) beyond location 2. It is indeed striking that a very similar dispersed phase

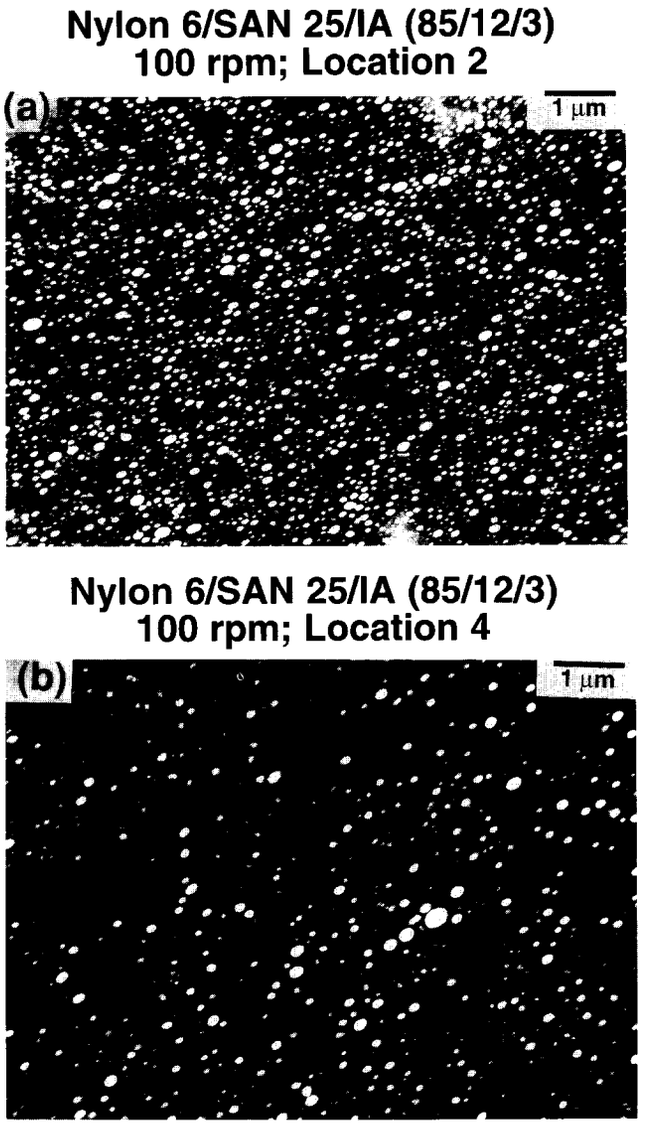

Figure 17 TEM photomicrographs of nylon 6/SAN 25/IA (85/12/3) blend samples taken from (a) location 2, $\bar{d}_w = 0.20\,\mu$m and (b) location 4, $\bar{d}_w = 0.19\,\mu$m of the clamshell extruder at a screw speed of 100 rpm and extruder configuration A

particle size is obtained at location 1 for binary and ternary blends in this series with 0.5 MA in the dispersed phase even though there is a dramatically different extent of reaction (see *Figures 24* and *25*). While most of the amine–anhydride reaction is complete at location 1 for the ternary blend, only 5% of the amine end-groups have reacted at this location for the binary blend. For the latter, the reaction appears to proceed continuously along the screw to its maximum limit (~30%) near the exit of the extruder. The pronounced coalescence observed in the ternary blends is no doubt related to the fact that this blend is subjected to high rheological stresses downstream in the kneading sections of the extruder after most of the amine–anhydride reaction is complete. In fact, it is possible that mechanisms similar to that suggested for compatibilized nylon 6/SAN blends also prevail in this case, i.e. in the ternary blend, the SEBS and SEBS-*g*-MA-2% fractions of the rubber phase become segregated due to stress and possibly thermodynamic causes as the maleic anhydride units react with the polyamide

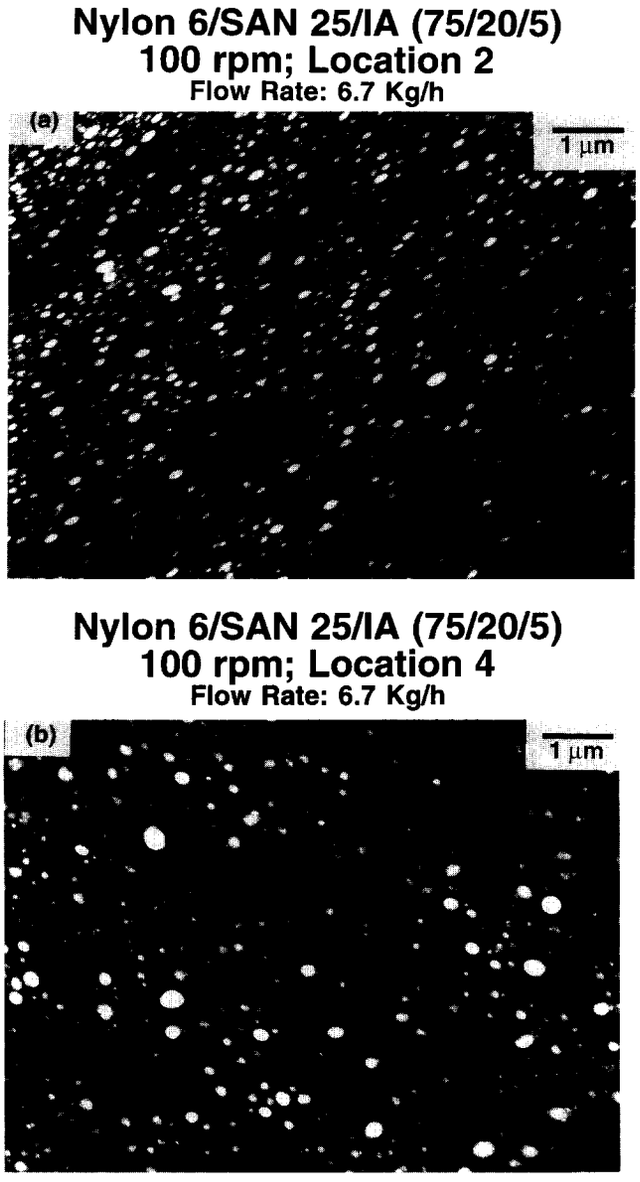

Figure 18 TEM photomicrographs of nylon 6/SAN 25/IA (75/20/5) blend samples taken from (a) location 2, $\bar{d}_w = 0.23\,\mu m$ and (b) location 4, $\bar{d}_w = 0.29\,\mu m$ of the clamshell extruder with an increased flow rate of $6.7\,kg\,h^{-1}$ at a screw speed of 100 rpm and extruder configuration A

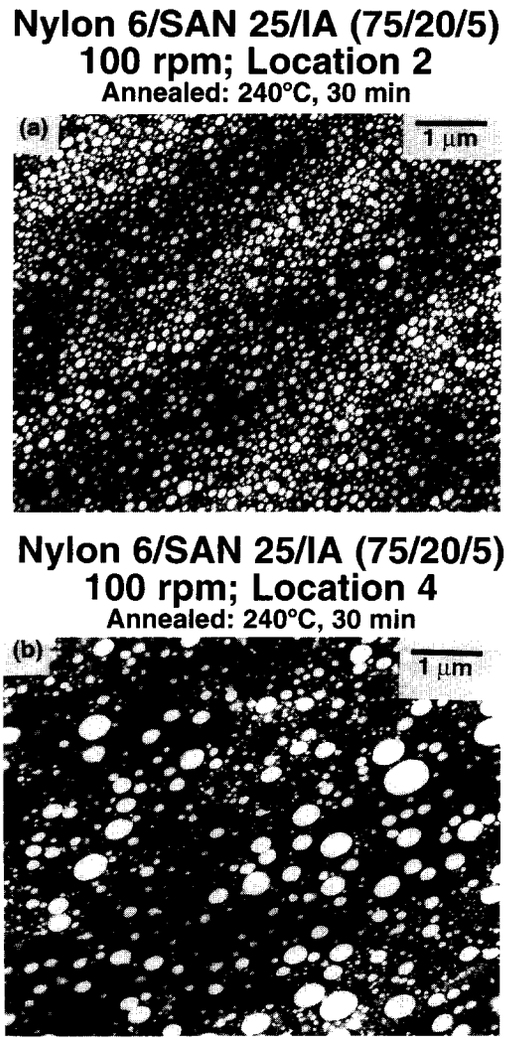

Figure 19 TEM photomicrographs of nylon 6/SAN 25/IA (75/20/5) blend samples annealed under inert nitrogen purge for 30 min at 240°C after taken from (a) location 2, $\bar{d}_w = 0.15$ and (b) location 4, $\bar{d}_w = 0.32$ of the clamshell extruder operating at 100 rpm

chains. Segregation of the graft copolymer from the SEBS would generate particles without grafted chains which would be more susceptible to coalescence.

CONCLUSIONS

The patterns of morphology generation observed here for non-reactive blends are consistent with other investigations; however, some novel observations are described for reactively compatibilized systems. Depending on composition and mixing conditions employed, coalescence of dispersed phase particles was observed downstream along the screw for two reactive polyamide systems investigated. The onset and extent of coalescence in these blends depends on a number of different variables which are often interrelated, including screw speed, screw geometry, feed rate, rate of progression of reaction along extruder screw, concentration of the dispersed phase and availability of functional groups. While higher screw speed facilitates rapid melting of the extrudate and faster consumption of the reactive groups in the initial regions of the screw, it can also promote coalescence downstream along the screw. The introduction of more intensive mixing elements in the form of kneading blocks downstream along the screw can shift the balance between drop break-up and coalescence to favour the latter. While it is unlikely that dynamic equilibrium is attained at any point along the screw for the reactively compatibilized blends investigated here, their morphological stability during quiescent annealing in the melt indicates the necessity of dynamic forces (e.g. shear and extensional stresses) for affecting any change in morphology of these systems. This also indicates that in reactively compatibilized blends a higher concentration of copolymer chains per unit area may be required for providing effective steric stabilization of the dispersed phase particles against coalescence in a flow type situation as opposed to quiescent conditions. This phenomenon is similar to recent observations by

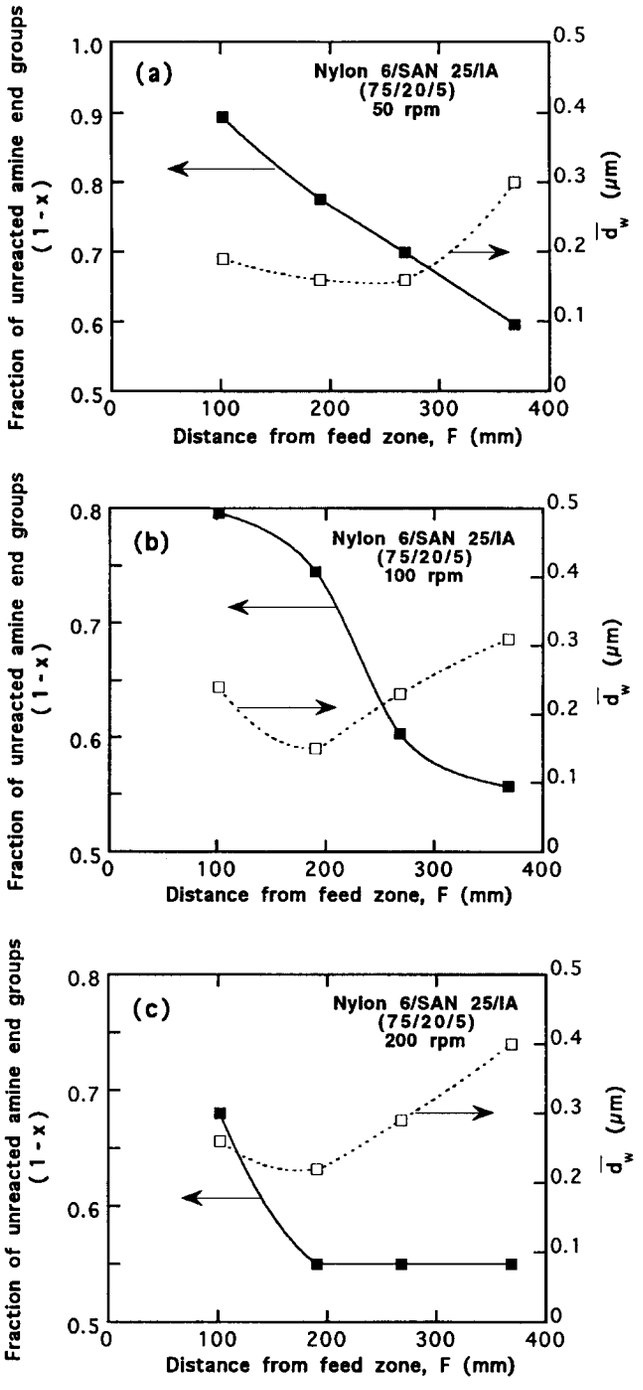

Figure 20 Fraction of unreated amine end groups and dispersed phase particle size vs distance from the feed zone for nylon 6/SAN 25/IA (75/20/5) blends at screw speeds of (a) 50 rpm; (b) 100 rpm; and (c) 200 rpm

Sondergaard and Lyngaae-Jorgensen in PS/PMMA systems compatibilized by a PS-PMMA block copolymer[52,53].

It is obvious from this study that some of the same factors which are intuitively believed to increase the efficiency of mixing in polymer blends could have an opposite effect on reactively compatibilized systems where the dispersed phase is more finely dispersed. More intensive mixing, after the minimum particle size has been attained, can lead to coalescence of the dispersed phase particles to form significantly larger

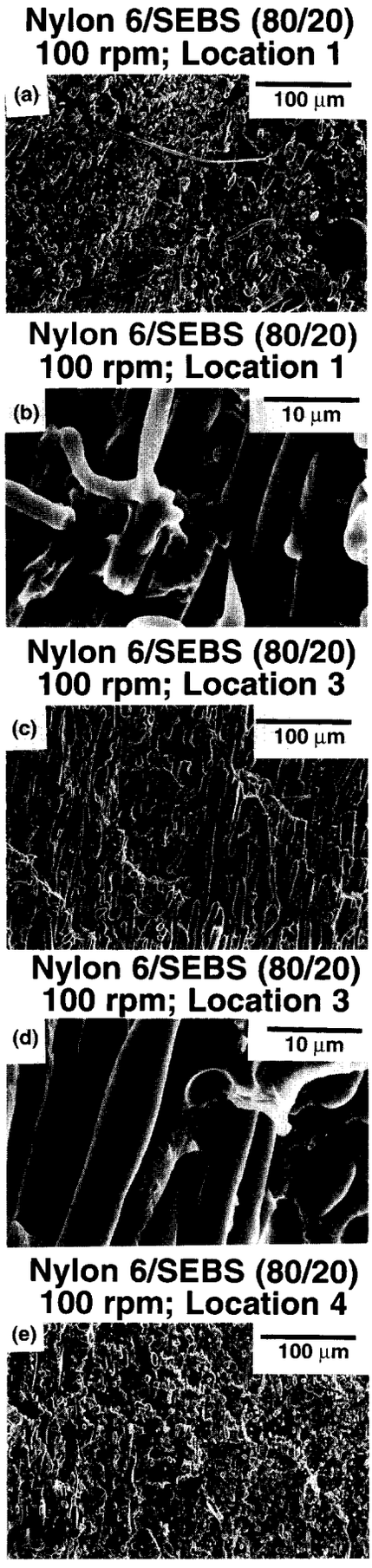

Figure 21 SEM photomicrographs for nylon 6/SEBS (80/20) blends at (a) location 1; (b) location 1, at a higher magnification; (c) location 3; (d) location 3, at higher magnification; and (e) location 4 at a screw speed of 100 rpm and extruder configuration A

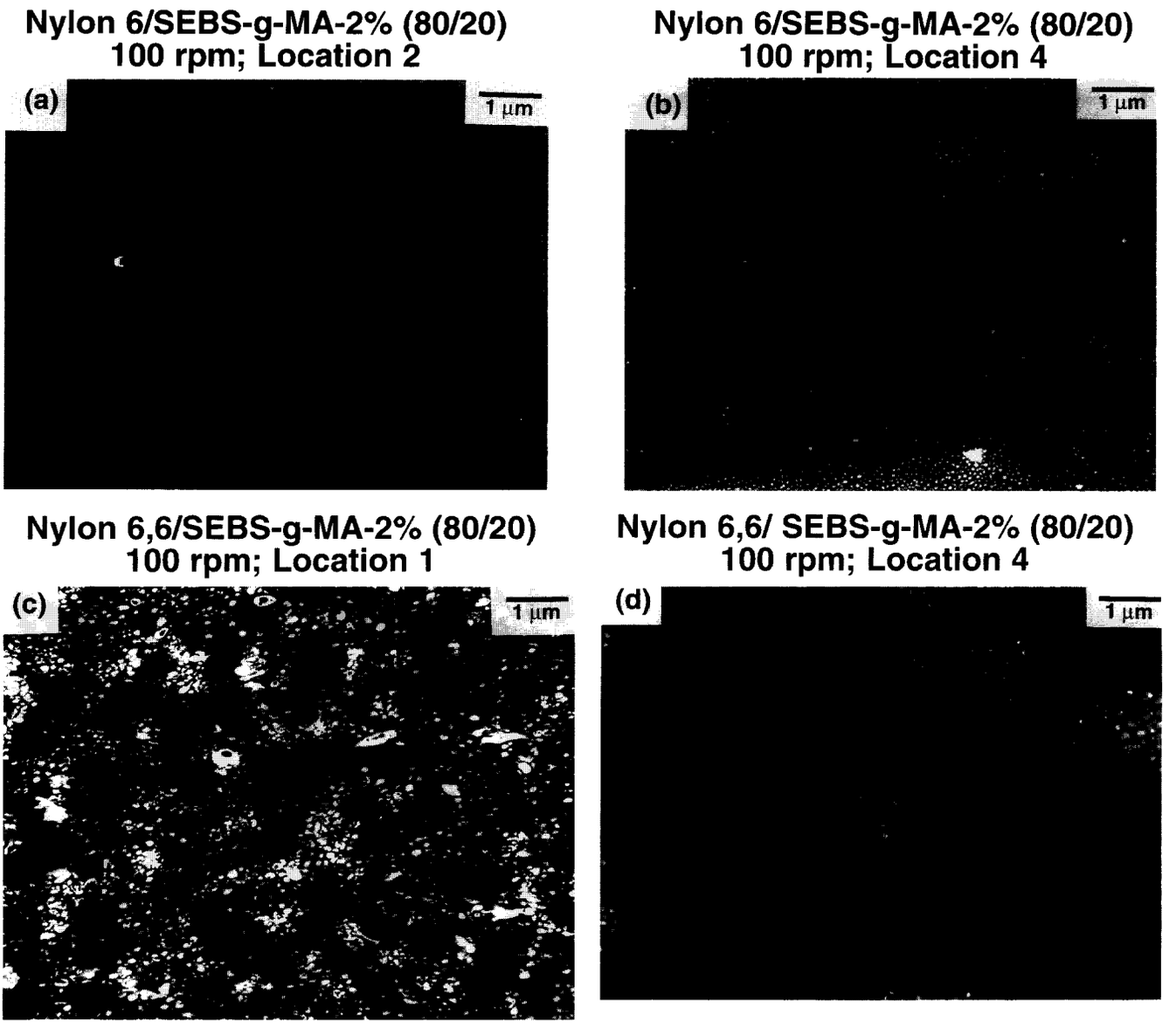

Figure 22 TEM photomicrographs of nylon 6/SEBS-*g*-MA-2% (80/20) blend at (a) location 2 and (b) location 4; and of nylon 6,6/SEBS-*g*-MA-2% (80/20) blend at (c) location 2 and (d) location 4 at a screw speed of 100 rpm and extruder configuration A

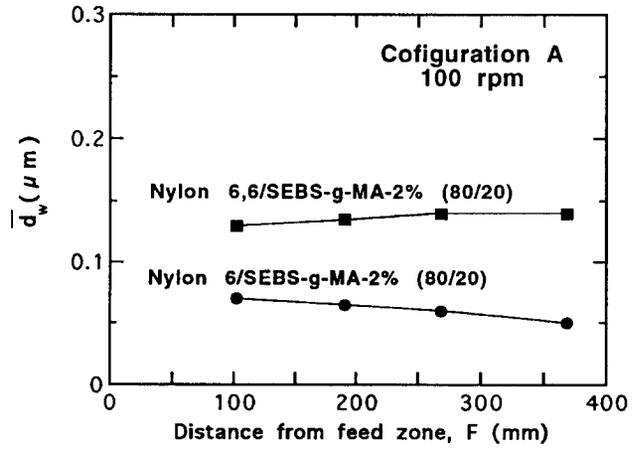

Figure 23 Dispersed phase particle size as a function of the distance from the feed zone of the clamshell extruder for SEBS-*g*-MA-2% blends with nylon 6 and nylon 6,6 at a screw speed of 100 rpm and extruder configuration A

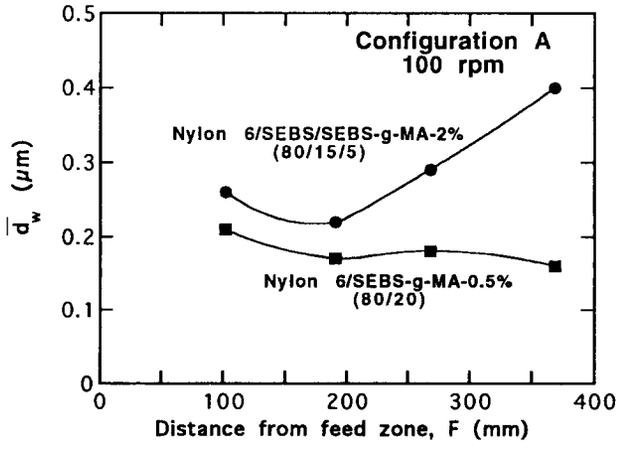

Figure 24 Dispersed phase particle size as a function of the distance from the feed zone of the clamshell extruder for nylon 6/SEBS/SEBS-*g*-MA-2% (80/15/5) and nylon 6/SEBS-*g*-MA-0.5% blends as computed from TEM photomicrographs

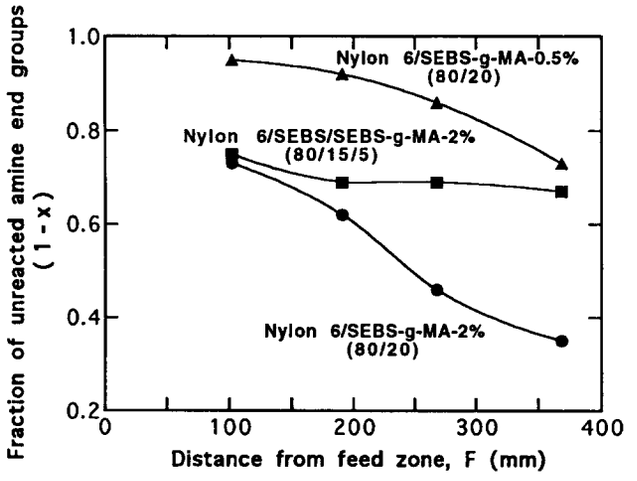

Figure 25 Fraction of untreated amine end groups vs distance from the feed zone for nylon 6/SEBS-*g*-MA-2% (80/20), nylon 6/SEBS-*g*-MA-0.5% (80/20) and nylon 6/SEBS/SEBS-*g*-MA-2% (80/15/5) blends

domains. In a typical processing type situation where morphology of the blend is often examined only at the exit of the extruder such dramatic variations of morphology downstream along the extruder screw could be easily overlooked. This could dramatically change the ultimate mechanical properties of the blends of semicrystalline polymers sensitive to small variations in morphology.

ACKNOWLEDGEMENTS

The authors are grateful to D. J. Dufesne for assistance with processing experiments and to 3M Company for permission to publish this work. This research was also partially supported by the US Army Research Office.

REFERENCES

1 Paul, D. R., Barlow, J. W. and Keskkula, H. in 'Encyclopedia of Polymer Science and Engineering' (Eds H. Mark, N. Bikales, C. G. Overberger and H. Menges), 2nd Edn, Vol. 12, Wiley-Interscience, New York, 1988, p. 399
2 Paul, D. R. in 'Thermoplastic Elastomers: Research and Development' (Eds N. R. Legge, H. Schroeder and G. Holden), Hanser Verlag, Munich, 1987, Ch. 12, Section 6
3 Teyssie, P. *Makromol. Chem., Macromol. Symp.* 1988, **22**, 83
4 Sjoerdsma, S. D., Bleijenberg, A. C. A. M. and Heikens, D. *Polymer* 1981, **22**, 619
5 Paul, D. R. in 'Functional Polymers' (Eds D. E. Bergbreiter and C. E. Martin), Plenum Press, New York, 1989, p. 1
6 Majumdar, B., Keskkula, H., Paul, D. R. and Harvey, N. G. *Polymer* 1994, **35**, 4263
7 Triacca, V. J., Ziaee, S., Barlow, J. W., Keskkula, H. and Paul, D. R. *Polymer* 1992, **32**, 1401
8 Majumdar, B., Keskkula, H. and Paul, D. R. *Polymer* 1994, **35**, 3164
9 Majumdar, B., Keskkula, H. and Paul, D. R. *Polymer* 1994, **35**, 5453, 5468
10 Majumdar, B., Keskkula, H. and Paul, D. R. *Polymer* 1994, **35**, 1386
11 Majumdar, B., Keskkula, H. and Paul, D. R. *Polymer* 1994, **35**, 1399
12 Oshinski, A. J., Keskkula, H. and Paul, D. R. *Polymer* 1992, **33**, 268; 284
13 Takeda, Y., Keskkula, H. and Paul, D. R. *Polymer* 1992, **33**, 3173
14 Padwa, A. R. and Lavengood, R. E. *ACS Symp. Ser.* 1992, **33**, 600
15 Hallden-Abberton, M. *Polym. Mater. Sci. Eng.* 1991, **65**, 361
16 Fowler, M. E., Paul, D. R., Cohen, L. A. and Freed, W. T. *J. Appl. Polym. Sci.* 1989, **7**, 513
17 Hallden-Abberton, M., Bortnick, N., Chen, L., Freed, W. and Fromuth, H. US Patent 4954574, 1990
18 Taylor, G. I. *Proc. R. Soc. London* 1932, **A138**, 41
19 Taylor, G. I. *Proc. R. Soc. London* 1934, **A146**, 501
20 von Smoluchowski, M. *Physik. Z.* 1916, **17**, 557, 585
21 von Smoluchowski, M. *Z. Physik. Chem.* 1917, **92**, 129
22 Bartok, W. and Mason, S. G. *J. Colloid Sci.* 1958, **13**, 393
23 Bartok, W. and Mason, S. G. *J. Colloid Sci.* 959, **14**, 13
24 Rumscheidt, F. D. and Mason, S. G. *J. Colloid Sci.* 1961, **16**, 238
25 Torza, S., Cox, R. C. and Mason, S. G. *J. Colloid Interface Sci.* 1972, **38**, 395
26 Choi, S. J. and Schowalter, W. R. *Phys. Fluids* 1975, **18**, 420
27 van Oene, H. *J. Colloid Interface Sci.* 1972, **40**, 448
28 Karam, H. J. and Bellinger, J. C. *Ind. Eng. Chem. Fundam.* 1986, **167**, 241
29 Grace, H. P. *Chem. Eng. Commun.* 1982, **14**, 225
30 Acrivos, A. and Lo, T. S. *J. Fluid Mech.* 1978, **86**, 641
31 Han, C. D. and Funatsu, K. *J. Rheol.* 1978, **22**, 113
32 Flumerfelt, R. W. *Ind. Eng. Chem. Fundam.* 1972, **11**, 312
33 Flumerfelt, R. W. *J. Colloid Interface Sci.* 1980, **76**, 33
34 Chin, H. B. and Han, C. D. *J. Rheol.* 1979, **23**, 557
35 Chin, H. B. and Han, C. D. *J. Rheol.* 1980, **24**, 1
36 Han, C. D. 'Multiphase Flow in Polymer Processing', Academic Press, New York, Academic Press, 1981
37 Wu, S. *Polym. Eng. Sci.* 1987, **27**, 335
38 Serpe, G., Jarrin, J. and Dawans, F. *Polym. Eng. Sci.* 1990, **30**, 553
39 Chesters, A. K. *Trans. IChemE* 1991, **69**, 259
40 Abid, S. and Chesters, A. K. *Int. J. Multiphase Flow* 1994, **20**, 613
41 Chesters, A. K. and Hoffman, G. *Appl. Sci. Res.* 1982, **38**, 353
42 Ramakrishna, D. *Rev. Chem. Eng.* 1985, **3**, 49
43 Tokita, N. *Rubber Chem. Technol.* 1977, **50**, 292
44 Elmendorp, J. J. and Van der Vegt, A. K. *Polym. Eng. Sci.* 1986, **26**, 418
45 Fortelny, I. and Zivny, A. *Polymer* 1995, **36**, 4113
46 Fortelny, I., Kamenicka, D. and Kovar, J. *Angew. Makromol. Chem.* 1988, **1664**, 125
47 Fortelny, I. and Kovar, J. *Eur. Polym. J.* 1989, **25**, 317
48 Fortelny, I. and Kovar, J. *Polym. Compos.* 1988, **9**, 119
49 Fortelny, I. and Zivny, A. *Polym. Eng. Sci.* 1995, **35**, 1872
50 Fortenly, I. and Zivny, A. *Polymer* 1995, **21**, 4113
51 Lyngaae-Jorgensen, J. and Utracki, L. A. *Makromol. Chem., Macromol. Symp.* 1991, **48/49**, 189
52 Sondergaard, K. and Lyngaae-Jorgensen, J. in 'Rheo-Physics of Multiphase Systems: Characterization by Rheo-Optical Techniques' (Eds K. Sondergaard and J. Lyngaae-Jorgensen), Technomic Publishing Co., Lancaster, PA, 1995
53 Sondergaard, K. and Lyngaae-Jorgensen, J. in 'Flow-induced Structure in Polymers' (Eds A. I. Nakatani and M. D. Dadmun), American Chemical Society, Washington DC, 1995
54 Ultracki, L. A. and Shi, Z. H. *Polym. Eng. Sci.* 1992, **32**, 1824
55 Bordereau, V., Shi, Z. H., Utracki, L. A., Sammut, P. and Carrega, M. *Polym. Eng. Sci.* 1992, **32**, 1846
56 Huneault, M. A., Shi, Z. H. and Utracki, L. A. *Polym. Eng. Sci.* 1995, **35**, 115
57 Roland, C. M. and Bohm, G. G. A. *J. Polym. Sci., Polym. Phys. Edn* 1984, **28**, 2011
58 Sundararaj, U. and Macosko, C. W. *Macromolecules* 1995, **28**, 2647
59 Favis, B. D. and Chalifoux, J. P. *Polym. Eng. Sci.* 1987, **27**, 1591
60 Favis, B. D. and Willis, J. M. *J. Polym. Sci., Part B. Polym. Phys.* 1990, **28**, 2259
61 Willis, J. M., Caldas, V. and Favis, B. D. *J. Mater. Sci.* 1991, **26**, 4742
62 Favis, B. D. *Polymer* 1994, **35**, 1552
63 Oshinski, A. J., Keskkula, H. and Paul, D. R. *Polymer* 1996, **37**, 4891
64 Meier, D. J. *J. Phys. Chem.* 1967, **71**, 1861
65 Molau, G. E. in 'Block Copolymers' (Ed. S. L. Aggarwal), Plenum Press, New York, 1970, p. 70
66 Reiss, G., Kohler, J., Tournut, C. and Brandert, A. *Makromol. Chem.* 1967, **101**, 58
67 Rudin, R. J. *Rev. Makromol. Chem.* 1980, **C19**, 267
68 Anastasiadis, S. H., Gancarz, I. and Koberstein, J. T. *Macromolecules* 1989, **22**, 1449

69 Shull, K. A. and Kramer, E. J. *Macromolecules* 1990, **23**, 45769
70 Shull, K. R., Kramer, E. J., Hadziioannou, G. and Tang, W. *Macromolecules* 1990, **23**, 4780
71 Fleicher, C. A., Koberstein, J. T., Krukonis, V. and Wetmore, P. A. *Macromolecules* 1993, **26**, 4172
72 Wagner, M. and Wolf, B. A. *Polymer* 1993, **34**, 1460
73 Tang, T. and Huang, B. *Polymer* 1994, **35**, 281
74 Hu, W., Koberstein, J. T., Lingelser, J. P. and Gallot, Y. *Macromolecules* 1995, **8**, 5209
75 Noolandi, J. and Hong, K. M. *Macromolecules* 1982, **15**, 482
76 Leibler, L. *Makromol. Chem., Macromol. Symp.* 1988, **16**, 1
77 Wang, Z. G. and Safran, S. A. *J. Phys. France* 1990, **51**, 185
78 Freed, K. F. and Dudowicz, J. *Pure Appl. Chem.* 1995, **67**, 969
79 Dolan, A. K. and Edwards, S. F. *Proc. Roy. Soc. A* 1974, **337**, 509
80 Dolan, A. K. and Edwards, S. F. *Proc. Roy. Soc. A* 1975, **343**, 427
81 Gerber, P. R. and Moore, M. A. *Macromolecules* 1977, **10**, 476
82 De Gennes, P.-G. 'Scaling Concepts in Polymer Physics', Cornell, Ithaca, New York, 1979
83 De Gennes, P. G. *J. Phys. (Paris)* 1976, **37**, 1443
84 Alexander, S. *J. Phys. (Paris)* 1977, **38**, 977; 983
85 Smitham, J. B. and Napper, D. H. *J. Colloid Interface Sci.* 1976, **54**, 467
86 Smitham, J. B. and Napper, D. H. *J. Chem. Soc., Faraday Trans I* 1976, **72**, 2425
87 Watanabe, H. and Tirrell, M. *Macromolecules* 1993, **26**, 6455
88 Milner, S. T. *Science* 1991, **251**, 905
89 Pincus, P. *Macromolecules* 1991, **24**, 2912
90 Djakovic, L., Dokic, P., Radivojevic, P., Sefer, I. and Sovilj, V. *Colloid Polym. Sci.* 1987, **265**, 993
91 Walstra, P. in 'Encyclopedia of Emulsion Technology' (Ed. P. Becher), Marcel Dekker Inc., New York, 1983, p. 57
92 Karger-Kocsis, J., Kallo, A. and Kuleznev, V. N. *Polymer* 1984, **25**, 279
93 Plochocki, A. P., Dagli, S. S. and Andrews, R. D. *Polym. Eng. Sci.* 1989, **29**, 617
94 Schreiber, H. P. and Olguin, A. *Polym. Eng. Sci.* 1983, **23**, 129
95 Scott, C. E. and Macosko, C. W. *Polymer* 1994, **35**, 5422
96 Scott, C. E. and Macosko, C. W. *Intern. Polymer Processing X* 1995, **1**, 36
97 Scott, C. E. and Macosko, C. W. *Polymer* 1995, **36**, 461
98 Jang, B. Z., Uhlman, D. R. and Van der Sande, J. B. *Rubber Chem. Technol* 1984, **57**, 291
99 Sundararaj, U. T., Macosko, C. W., Rolando, R. J. and Chan, H. T. *Polym. Eng. Sci.* 1992, **32**, 1814
100 Maier, C., Lambla, M. and Ilham, K. *SPE ANTEC '95* 1995, 2015
101 Chan, H. T. and Dufresne, D. A. *SPE ANTEC '95* 1995, 302
102 Eise, K., Curry, J. and Nangeroni, J. F. *Polym. Eng. Sci.* 1983, **23**, 642
103 Lim, S. and White, J. L. *Intern. Polymer Processing VIII* 1993, **2**, 119
104 Chen, C. C., Fontan, E., Min, K. and White, J. L. *Polym. Eng. Sci.* 1988, **28**, 69
105 De Loor, A., Cassagnau, P., Michel, A. and Vergnes, B. *Intern. Polymer Processing IX* 1994, **3**, 211
106 Anradi, L. N. and Helman, G. P. *Polym. Eng. Sci.* 1995, **35**, 693
107 Nishio, T., Suzuki, Y., Kojima, K. and Kakugo, M. *J. Polym. Eng.* 1991, **10**, 123
108 Majumdar, B., Keskkula, H. and Paul, D. R. *J. Appl. Polym. Sci.* 1994, **54**, 339
109 Polance, R. and Jayaraman, K. *Polym. Eng. Sci.* 1995, **35**, 1535
110 Epstein, B. N. US Patent 4,174,358, issued to DuPont, 1979
111 Cimmino, C., D'Orazio, L., Greco, R., Maglio, G., Malinconico, C., Mancarella, C., Martusceli, E., Palumbo, R. and Ragosta, G. *Polym. Eng. Sci.* 1984, **24**, 48
112 Borggreve, R. J. M., Gaymans, R. J., Scuijer, J. and Ingen Housz, J. F. *Polymer* 1987, **28**, 1489
113 Borggreve, R. J. M. and Gaymans, R. J. *Polymer* 1989, **30**, 63
114 Gaymans, R. J. and Borggreve, R. J. M. in 'Contemporary Topics of Polymer Science' (Ed. B. M. Culbertson), Vol. 6, Plenum Press, New York, 1990, p. 461
115 Oshinski, A. J., Keskkula, H. and Paul, D. R. *Polymer* 1996, **37**, 4409 and 4919